DISSERTATIONES
PHYSICAE
UNIVERSITATIS
TARTUENSIS
113

HARDI VEERMÄE

Dark matter with long range vector-mediated interactions

DISSERTATIONES PHYSICAE UNIVERSITATIS TARTUENSIS
113

DISSERTATIONES PHYSICAE UNIVERSITATIS TARTUENSIS
113

HARDI VEERMÄE

Dark matter with long range vector-mediated interactions

UNIVERSITY OF TARTU
Press

This study was carried out at the National Institute of Chemical Physics and Biophysics, Tallinn, and the University of Tartu, Estonia.

The dissertation was admitted on 05.09.2017 in partial fulfilment of the requirements for the degree of Doctor of Philosophy in physics, and was allowed for defence by the Council of the Institute of Physics, University of Tartu.

Supervisors: Dr. Emidio Gabrielli
National Institute of Chemical Physics and Biophysics,
Tallinn, Estonia

Dr. Stefan Groote
University of Tartu,
Tartu, Estonia

Dr. Martti Raidal
National Institute of Chemical Physics and Biophysics,
Tallinn, Estonia

Opponents: Dr. Oleg Lebedev
University of Helsinki,
Helsinki, Finland

Dr. Enn Saar
Tartu Observatory,
Tartu, Estonia

The public defence will take place on 27.10.2017 in the Institute of Physics, University of Tartu, W. Ostwaldi Str. 1.

ISSN 1406-0647
ISBN 978-9949-77-555-2 (print)
ISBN 978-9949-77-556-9 (pdf)

University of Tartu Press
www.tyk.ee

Contents

List of original publications

Publications related to the thesis

I. E. Gabrielli, L. Marzola, M. Raidal and H. Veermäe, "Dark matter and spin-1 milli-charged particles," JHEP **1508**, 150 (2015) [arXiv:1507.00571 [hep-ph]].

II. E. Gabrielli, L. Marzola, E. Milotti and H. Veermäe, "Polarization observables for millicharged particles in photon collisions," Phys. Rev. D **94**, no. 9, 095014 (2016), Erratum: Phys. Rev. D **95** no.11, 119903 (2017) [arXiv:1604.00393 [hep-ph]].

III. M. Heikinheimo, M. Raidal, C. Spethmann and H. Veermäe, "Dark matter self-interactions via collisionless shocks in cluster mergers," Phys. Lett. B **749**, 236 (2015) [arXiv:1504.04371 [hep-ph]].

IV. C. Spethmann, B. Deshev, M. Heikinheimo, A. Hektor, M. Raidal, T. Sepp and H. Veermäe, "Simulations of Galaxy Cluster Collisions with a Dark Plasma Component," [arXiv:1603.07324 [astro-ph.CO]]. Accepted for publication in Astronomy & Astrophysics after a revision.

Author's contribution to the publications

In publication I, the dissertant developed the model and performed all the calculations.

In publication II, the dissertant performed the calculations of the polarised cross-sections.

In publication III, the dissertant was involved in all aspects of the paper.

In publication IV, the dissertant provided the theoretical background and made contributions to the initial conditions code.

Other publications

V. S. Groote, H. Veermäe and C. Beck, "Short chaotic strings and their behaviour in the scaling region," Chaos Solitons Fractals **41** (2009) [arXiv:0803.2991 [nlin.CD]].

VI. S. Groote, H. Veermäe and C. Beck, "Renormalization group approach to chaotic strings," Chaos Solitons Fractals **53** (2013) 18 [arXiv:1208.1107 [nlin.CD]].

VII. E. Gabrielli, A. Racioppi, M. Raidal and H. Veermäe, "Implications of effective axial-vector coupling of gluon for $t\bar{t}$ spin polarizations at the LHC," Phys. Rev. D **87** (2013) no.5, 054001 [arXiv:1212.3272 [hep-ph]].

VIII. E. Gabrielli, M. Heikinheimo, L. Marzola, B. Mele, C. Spethmann and H. Veermäe, "Anomalous Higgs-boson coupling effects in HWW production at the LHC," Phys. Rev. D **89** (2014) no.5, 053012 [arXiv:1312.4956 [hep-ph]].

IX. A. Hektor, L. Marzola, M. Raidal and H. Veermäe, "A new mechanism for dark energy: the adaptive screening," JHEP **1501** (2015) 101

X. E. Gabrielli, K. Kannike, B. Mele, M. Raidal, C. Spethmann and H. Veermäe, "A SUSY Inspired Simplified Model for the 750 GeV Diphoton Excess," Phys. Lett. B **756** (2016) 36 [arXiv:1512.05961 [hep-ph]].

XI. L. Marzola, A. Racioppi, M. Raidal, F. R. Urban and H. Veermäe, "Non-minimal CW inflation, electroweak symmetry breaking and the 750 GeV anomaly," JHEP **1603** (2016) 190 [arXiv:1512.09136 [hep-ph]].

XII. E. Babichev, L. Marzola, M. Raidal, A. Schmidt-May, F. Urban, H. Veermäe and M. von Strauss, "Bigravitational origin of dark matter," Phys. Rev. D **94** (2016) no.8, 084055 [arXiv:1604.08564 [hep-ph]].

XIII. E. Babichev, L. Marzola, M. Raidal, A. Schmidt-May, F. Urban, H. Veermäe and M. von Strauss, "Heavy spin-2 Dark Matter," JCAP **1609** (2016) no.09, 016 [arXiv:1607.03497 [hep-th]].

XIV. H. Veermäe and M. Patriarca "Diffusion in the presence of a local attracting factor: Theory and interdisciplinary applications," Phys. Rev. E **95** (2017) 062116 [arXiv:1603.07102]

XV. K. Kannike, M. Raidal, C. Spethmann and H. Veermäe, "Evolving Planck Mass in Classically Scale-Invariant Theories," JHEP **1704** (2017) 026 [arXiv:1610.06571 [hep-ph]].

XVI. M. Raidal and H. Veermäe, "On the Quantisation of Complex Higher Derivative Theories and Avoiding the Ostrogradsky Ghost," Nucl. Phys. B **916** (2017) 607
[arXiv:1611.03498 [hep-th]].

XVII. L. Järv, K. Kannike, L. Marzola, A. Racioppi, M. Raidal, M. Rünkla, M. Saal and H. Veermäe, "A frame independent classification of single field inflationary models," Phys. Rev. Lett. **118** (2017) no.15, 151302 [arXiv:1612.06863 [hep-ph]].

XVIII. B. Carr, M. Raidal, T. Tenkanen, V. Vaskonen and H. Veermäe, "Primordial black hole constraints for extended mass functions," Phys. Rev., D **96** (2017) no.2, 023514 [arXiv:1705.05567 [astro-ph.CO]].

XIX. K. Kannike, L. Marzola, M. Raidal and H. Veermäe, "Single Field Double Inflation and Primordial Black Holes," [arXiv:1705.06225 [astro-ph.CO]]. Accepted for publication in JCAP.

XX. M. Raidal, V. Vaskonen and H. Veermäe, "Gravitational Waves from Primordial Black Hole Mergers," [arXiv:1707.01480 [astro-ph.CO]]. Accepted for publication in JCAP.

XXI. M. Heikinheimo, K. Kannike, F. Lyonnet, M. Raidal, K. Tuominen and H. Veermäe, "Vacuum Stability and Perturbativity of SU(3) Scalars," [arXiv:1707.08980 [hep-ph]]. Accepted for publication in JHEP.

1 Introduction

The nature of dark matter (DM) is considered to be one of the great problems of contemporary physics. Most of our current knowledge of the fundamental laws of the observable Universe from the smallest accessible scales to the largest observable distances can be summed up by two standard models. The Standard Model of particle physics (SM) [1] comprises 3 generations of elementary fermions, the quarks and the leptons, and the mediators of the fundamental interactions including the Higgs boson. The standard model of cosmology dubbed ΛCDM tells us that the majority, roughy 70%, of the mass-energy density the Universe is carried by the cosmological constant (Λ), which is responsible for the accelerating expansion, while the rest of comprises matter [2]. Only a sixth of the matter component can be accounted for by the Standard Model particles; the rest, that is cold dark matter (CDM), is presently observed only through its gravitational interaction. Decades of dedicated experiments have revealed little about its nature, besides the fact that, if it interacts with visible matter, then the interaction must be extremely weak [3, 4].

Strong observational evidence for the existence of DM is provided by the rotation curves of galaxies, the power spectrum of temperature fluctuations of the cosmic microwave background (CMB) and gravitational lensing experiments. One of the most interesting experimental pieces to the puzzle of the nature of DM come from astrophysical observations of a small number of galaxy cluster collisions. They alone strongly favour the hypothesis that DM is some kind of a substance rather than a modification of the gravitational interaction. The best known example of these rare events is probably the Bullet Cluster. It was formed by a collision of two clusters with masses roughly ten times different. As the smaller cluster, the "bullet", moved through the larger one at roughly 4700 km/s the intracluster gas interacted and left behind a prominent bow shock composed of hot X-ray emitting gas [5–7]. Weak lensing analysis reveals a dark clump separated from the gas and the larger cluster implying that

the DM components had passed through each other indicating that all of DM can not be collisional.

Even the basic properties of DM can vary enormously. For example, in viable DM models its mass can range by 70 orders of magnitude. On the low mass end, at 10^{-23}eV [1] there is fuzzy DM, a coherent ultracold scalar field with a wavelength of the size of a dwarf galaxy. The heaviest DM particles are primordial black holes that could weigh thousands of solar masses, although they are current observations indicate that they can not make up all of DM [8, 9]. In the middle of the spectrum lives the weakly interacting massive particle (WIMP) which has so far been the most prominent DM candidate [3, 10, 11]. It has many desirable features: it is cold, almost non-interacting and appears naturally in supersymmetric extensions of the SM. The popularity of the WIMP has recently declined, however, because of the non-observation of supersymmetry in the Large Hardon Collider (LHC) and the null results of DM direct detection experiments.

The visible sector described by the SM has an incredibly rich phenomenology at any accessible energy scale. In sharp contrast to it, the DM of ΛCDM is quite plain as it can be perfectly described by a single particle species that is cold and non-interacting. This might not be the case, however. Even, if it has been established that the dark and visible sectors do practically not interact, it is still possible that the dark sector has a more interesting internal life. Observation of the Bullet Cluster [6, 12] and simulations of large scale structure formation [13, 14] can constrain the strength of the of DM self-interaction, yet they still allow self-interactions with strength comparable to the strong force. These constrains are weakened even more if the dark sector contains more than one particle species.

Although ΛCDM is in an excellent agreement with many astrophysical and cosmological observations it seems to be in conflict with several small-scale astrophysical puzzles such as the missing satellite problem [15, 16], the core-cusp problem [17,18] and the too-big-to-fail problem [19,20]. DM self-interactions are a possible solution to at least some of these problems [21, 22]. Moreover, the observation of a central clump in the Abell 520 galaxy cluster [23–26] is a direct hint of DM self-interaction. Al-

[1] In this thesis natural units $\hbar = c = k_B = 1$ are used.

though scenarios in which all of the DM is self interacting do not give the observed DM distribution of Abell 520 [24], it can be obtained within models in which only a subcomponent of DM is self-interacting [27, 28].

DM self-interactions can be divided into two broad categories. Short range interactions are characterised by hard collisions between particles. These usually imply the existence of a massive mediator whose inverse mass sets the range of the interaction. Long range interactions are thus mediated by massless or extremely light bosons. In this thesis various scenarios are considered where the dark sector contains particles with long range interactions mediated by a vector boson.

A natural candidate for such a boson is the photon, implying that the DM particles would be electrically charged. Scenarios containing such hidden charged particles are already severely constrained and dark particles with charges of the order of the elementary charged are ruled out unless they are very heavy [29–53]. In the SM the electric charge is quantized in units of 1/3 of the elementary charge[2] although there is no obvious theoretical reason for it. It could be a consequence of physics beyond the SM such as grand unified theories [54], and also the detection of magnetic monopoles would demand charge quantization [55]. Nevertheless, as this is not a requirement of nature, the particles of the dark sector could carry a tiny electric charge $\epsilon \ll 1$, dubbed milli-charge[3]. This milli-charge could be naturally acquired through radiative corrections in theories with additional $U(1)$ gauge interactions [56]. At the phenomenological level, milli-charged particles can be simply introduced by hand. Many constraints can be relaxed if the DM particles combine into neutral bound states [57–60]. Also, it has been argued that astrophysical magnetic fields could expel charged DM from the galactic disk which allows to evade the constraints from DM direct detection [48, 61].

The dark sector may also contain its own photon, a dark photon[4]. Such additional $U(1)$ interactions are, for example, predicted in string theory [64–71]. There exist scenarios where the dark photon itself (in this case it is necessarily massive) makes up the DM [72, 73]. In this

[2] In the rest of the thesis the electric charge will be expressed in units of the elementary charge e.

[3] Some authors prefer the term mini-charge.

[4] Dark photons are also referred to as hidden photons [62] or paraphotons [63] by some authors.

thesis we will consider only a massless dark photon mediating DM self-interactions [27, 74, 75].

A vector boson mediator implies that DM or a fraction of it can be in the plasma state [27]. For example, if the dark sector does not possess a particle–antiparticle asymmetry, then the charged DM particles naturally form a pair plasma. Because of the collective plasma effects the DM can be collisional even if the individual hard scattering events are negligible and thus counterstreaming DM could exhibit shocking behaviour. Studies of the Bullet Cluster imply that only a fraction of DM can be in such a state [6, 7]. If this were to be realised in nature its effect could be observable in collisions of DM haloes and explain the central mass clump in the Abell 520 cluster [27, 28].

The general aim of this thesis was to study the phenomenological aspects of models in which the dark sector contains interactions mediated by a massless $U(1)$ gauge boson. In the first two publications we studied the phenomenology of millicharged particles and the implications of their spin [76,77]. In particular, we constructed a minimal model for spin-1 millicharged particles [76]. In the last two publications the phenomenology of dark electromagnetism was considered with the emphasis on possible plasma effects and their implications on galaxy cluster mergers. In particular, we demonstrated that plasma instabilities alone can render dark matter collisional [27] and showed by a numerical simulation that, if a fraction of dark matter is collisional, then it is possible to reproduce the features observed in the Abell 520 cluster while satisfying the constraints from the Bulltet Cluster [28].

This thesis is structured as follows: In section 2 we present the theoretical background and the relevant experimental constraints for models containing extra $U(1)$ interactions or milli-charged particles of different spin. In section 3 we review the CDM paradigm and consider the cosmological applications of the models discussed in the previous section. These sections are intended to provide a preface to the publications the thesis is based on. In section 4 the results are summarised in English and in section 5 in Estonian. The publications on which this thesis is based on are presented in the appendix.

2 Hidden particles with $U(1)$ interactions

In this section we review the features of particles charged under a $U(1)$ gauge group with the emphasis on the spin of these particles. This gauge interaction may correspond to the electromagnetic force or to some unknown dynamics in the dark sector. We describe the generation of millicharge through kinetic and mass mixing.

2.1 Charged scalars, fermions and vectors

The SM is a gauge theory of the non-abelian gauge group $U(1) \times SU(2) \times SU(3)$. Gauge theories possess a beautiful and intricate geometric structure of which we will review only the relevant minimum.

2.1.1 Gauge theory basics

A gauge transformation of a field ψ that lives in a representation of a Lie group G is given by

$$\psi \mapsto U\psi, \tag{2.1}$$

where U is a field valued in the group G. It can be expressed as $U = \exp(ie\theta)$, where $\theta = \theta^a T_a$ is an arbitrary space-time dependent function valued in the Lie algebra of the gauge group, that is, it is a linear combination of the group generators T_a with space-time dependent coefficients. We assume here that G is compact and simple. The Lie algebra is determined by the commutation relations $[T_a, T_b] = i f_{abc} T_c$, where f_{abc} are the structure coefficients of the algebra. The parameter e is a coupling constant. To account for the locality of this transformation it is necessary to introduce the covariant derivative

$$D_\mu = \partial_\mu + ieA_\mu, \tag{2.2}$$

where $A_\mu = A_\mu^a T_a$ is a Lie algebra valued vector field. It acts as a connection on the field space and its transformation rules can be determined by requiring that the covariant derivative of the field ψ transforms covariantly, i.e. $D_\mu \psi \mapsto U D_\mu \psi$, as does the field itself. This implies

$$A_\mu \mapsto U A_\mu U^{-1} - (\partial_\mu U)\, U^{-1}. \tag{2.3}$$

The field tensor of the gauge group corresponds to the curvature $ieF_{\mu\nu} \equiv [D_\mu, D_\nu]$ and it transforms covariantly under the adjoint representation. From it the kinetic term or, in case of non-Abelian gauge groups, the Yang-Mills term

$$\mathcal{L}_{YM} = -\frac{1}{2} \operatorname{Tr}(F^{\mu\nu} F_{\mu\nu}) \tag{2.4}$$

can be constructed for the gauge fields. In the quantum theory it is necessary to add the gauge fixing and ghost terms

$$\mathcal{L}_{gf} = -\frac{1}{\xi} \operatorname{Tr}(\partial A)^2, \tag{2.5}$$

$$\mathcal{L}_{gh} = -\partial^\mu \bar{c} D_\mu c \tag{2.6}$$

to deal with the gauge degeneracy. The Faddeev–Popov ghost, $c \equiv c^a T_a$, is a fermionic scalar [78]. It does not appear in the physical spectrum. This choice of gauge fixing terms assumes a covariant gauge and gauge freedom to be partially preserved in the freedom to choose the gauge fixing parameter ξ. The Faddeev–Popov ghost decouples in Abelian theories ($f_{abc} = 0$) and enters non-Abelian theories only through loops. As we limit the discussion to tree level processes, it will be not relevant in the following.

In the following we focus mainly on the $U(1)$ gauge group. The general gauge transformation of the degrees of freedom ψ_i (the index i can stand for both internal and external degrees of freedom) carrying a charge q_i is given by

$$\psi_i \mapsto \exp(i q_i \theta) \psi_i, \tag{2.7}$$

together with $A_\mu \mapsto A_\mu - \partial_\mu \theta$, where θ is an arbitrary space-time dependent function. Throughout this section, the gauge field A_μ will be referred to as a photon for brevity, although it could as well correspond to a particle in the hidden sector, e.g. the dark photon or, in case the field is sufficiently massive, a Z'-boson.

Given a theory with a global symmetry under some group, this group can be easily gauged by the minimal substitution, that is, by making the replacement $\partial_\mu \to D_\mu$ in all derivative terms. The minimal substitution, however, will generally not yield the most general gauge invariant Lagrangian. The reason for this lies in the fact that the partial derivatives commute whereas the covariant derivatives do not. So, terms containing the field tensor $F_{\mu\nu} \propto [D_\mu, D_\nu]$, which is gauge *invariant* for abelian groups, would be absent from the Lagrangian to be gauged by minimal substitution. In the following we will separately treat the charged scalar, spinor and the vector field.

2.1.2 Models of charged particles for different spins

The simplest model of a charged particle is scalar quantum electrodynamics. It describes a fundamental charged scalar ϕ with the Lagrangian

$$\mathcal{L}_0 = |D\phi|^2 - m_\epsilon^2|\phi|^2 - \frac{\lambda}{4}|\phi|^4, \tag{2.8}$$

where m_ϵ denotes the mass of the scalar field and λ quantifies its self-interaction which we included for completeness.

It is possible that the mass term carries a opposite sign, $m_\epsilon^2 < 0$, in which case the field value at the minimum of the potential, i.e. the vacuum expectation value of the scalar, does not lie at the origin but at $v = m_\epsilon\sqrt{2/\lambda}$. Because the vacuum state is not symmetric under the gauge transformation, the symmetry is spontaneously broken and the photon acquires a mass. In detail, inserting the vacuum configuration $|\phi| = v$ into the Lagrangian (2.8) gives $\mathcal{L}_0 = e^2v^2A^\mu A_\mu + const.$ implying that the mass of the photon is $\sqrt{2}ev$. This way of generating the mass for a vector boson is known as the Higgs mechanism [79–81] and it is readily extended to the case when ϕ in (2.8) transforms under a non-Abelian gauge group. In the latter case some of the gauge symmetry, specifically the gauge subgroup leaving the vacuum state invariant, may be preserved.

Fundamental Dirac fermions ψ with mass m_ϵ obey the simple Lagrangian

$$\mathcal{L}_{1/2} = \bar{\psi}(i\not{D} - m_\epsilon)\psi. \tag{2.9}$$

As the fermion carries spin, it can have more complicated electromagnetic interactions, e.g. a magnetic moment. The tree level Lagrangian fixes

the gyromagnetic ratio to be $g = 2$. This value is modified by radiative corrections. The gyromagnetic ratio of the electron is measured with up to 12 decimal places which makes the fine structure constant one of the most precisely measured quantities. Its perfect agreement with the prediction of quantum electrodynamics makes it the most accurate physical theory to date [1].

The Lagrangians (2.8), (2.9) can be obtained by minimal substitution. However, this is not possible in the case of charged vector particles. In fact, minimal substitution predicts that the tree level gyromagnetic ratio of a charged vector boson is $g = 1$, yet unitarity arguments imply the value $g = 2$ [82]. Furthermore, a fundamental result of quantum theory is that unitary and renormalisable interactions between vectors must be gauge interactions [83–85]. As will be demonstrated in the next section, omitting mass terms, the Lagrangian of a fundamental charged (and thus complex) vector V_μ can be expressed as

$$\begin{aligned}\mathcal{L}_{V+EM} = &-\frac{1}{4}F_{\mu\nu}F^{\mu\nu} - \frac{1}{2}V_{\mu\nu}V^{\dagger\mu\nu} - ieF_3^{\mu\nu}V_\mu V_\nu^\dagger \\ &- \frac{e^2}{2}((V_\nu V^{\dagger\,\nu})^2 - |V_\nu V^\nu|^2),\end{aligned} \tag{2.10}$$

where $V_{\mu\nu} = D_\mu V_\nu - D_\nu V_\mu$ is the field tensor of the charged vector field V_μ after minimal substitution. The third term thus explicitly demonstrates that the electromagnetic interactions of V_μ are not obtained by the non-minimal substitution. Notably, the Lagrangian (2.10) contains a single parameter, the electric charge e, and is, in fact, a disguised $SU(2)$ Yang-Mills term. To make this explicit we can combine all vectors into another vector field valued in the Lie algebra of $SU(2)$,

$$\tilde{V}_\mu = \frac{1}{\sqrt{2}}(V_\mu + V_\mu^\dagger)T_1 + \frac{1}{i\sqrt{2}}(V_\mu - V_\mu^\dagger)T_2 + A_\mu T_3, \tag{2.11}$$

where T_i denote the generators of $SU(2)$ satisfying $[T_i, T_j] = i\epsilon_{ijk}T_k$. The Lagrangian (2.10) can now be rewritten as

$$\mathcal{L}_{V+EM} = -\frac{1}{2}\,\mathrm{Tr}\left(\tilde{V}^{\mu\nu}\tilde{V}_{\mu\nu}\right), \tag{2.12}$$

where $\tilde{V}^{\mu\nu} \equiv [(\partial + ie\tilde{V})_\mu, (\partial + ie\tilde{V})_\nu]/ie$ is the field tensor of the vector field $\tilde{V}_\mu$.

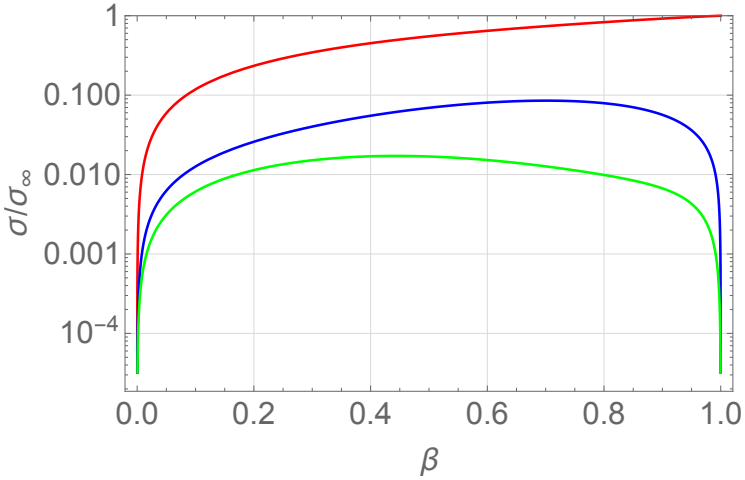

Figure 2.1: The unpolarised cross section for $S = 0$ (green), $S = 1/2$ (blue), $S = 1$ (red) in terms of the the velocity. Figure adapted from [77].

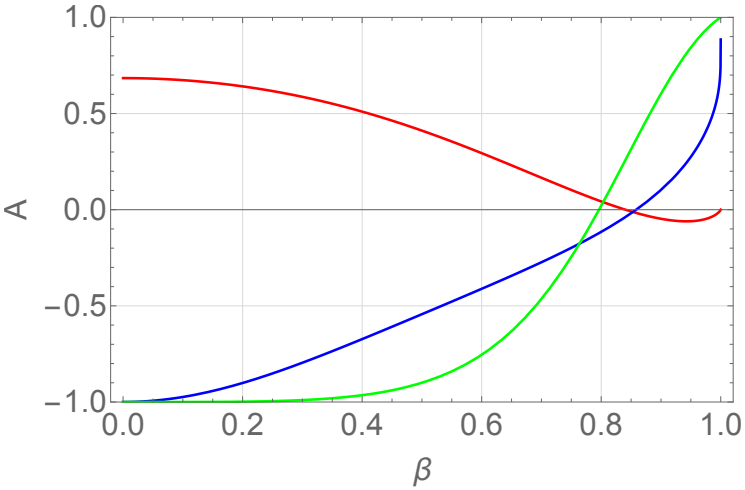

Figure 2.2: The polarisation asymmetry A for $S = 0$ (green), $S = 1/2$ (blue), $S = 1$ (red) in terms of the velocity. Figure adapted from [77].

To illustrate the effect of the variation of spin of the milli-charged particles consider their pair production in photon–photon collisions. In that case the mass for the vector milli-charged particles can now be added by hand without leading to violation of perturbative unitarity. When parity is conserved in these processes the polarised cross sections can be parametrised as

$$\sigma_{\gamma(h_1),\gamma(h_2)\to MCP,MCP} = \sigma(1 + Ah_1h_2), \tag{2.13}$$

where h_1, h_2 denote the helicities of the photons, σ is the unpolarised cross section and A a polarisation asymmetry. The unpolarised cross are depicted in Fig. 2.1 and the corresponding asymmetries in Fig. 2.2. The asymptotic behaviour of the unpolarised tree level cross sections for production of milli-charged particles with spin S are [77]

$$\sigma_{S=0}\big|_{\beta\to 0} = \frac{\sigma_\infty}{16}\beta, \qquad \sigma_{S=0}\big|_{\beta\to 1} = \frac{\sigma_\infty}{4}\frac{m_\epsilon^2}{s}, \tag{2.14}$$

$$\sigma_{S=1/2}\big|_{\beta\to 0} = \frac{\sigma_\infty}{8}\beta, \qquad \sigma_{S=1/2}\big|_{\beta\to 1} = \frac{\sigma_\infty}{2}\frac{m_\epsilon^2}{s}\ln\left(\frac{s}{m_\epsilon^2}\right), \tag{2.15}$$

$$\sigma_{S=1}\big|_{\beta\to 0} = \frac{19\sigma_\infty}{16}\beta, \qquad \sigma_{S=1}\big|_{\beta\to 1} = \sigma_\infty. \tag{2.16}$$

$$\sigma_{S=1,h=0}\big|_{\beta\to 0} = \frac{47\sigma_\infty}{240}\beta, \quad \sigma_{S=1,h=0}\big|_{\beta\to 1} = \frac{\sigma_\infty}{4}\frac{m_\epsilon^2}{s}. \tag{2.17}$$

where s is the square of the centre-of-mass energy of the process, $\beta \equiv \sqrt{1-4m_\epsilon/s}$ is the velocity of the milli-charged particles and

$$\sigma_\infty \equiv 8\pi\alpha^2\epsilon^4/m_\epsilon^2 \tag{2.18}$$

is a dimensional constant corresponding to the high energy asymptotic of the total cross section for the pair production of charged vectors ($S = 1$). For example, for the W-bosons $\sigma_\infty \approx 92$pb. Note that the high energy asymptotic for scalars (2.14) equals the high energy asymptotic for longitudinal vectors (2.17) as is expected from the Goldstone theorem [86]. An important difference here is that the asymptotic behaviour of the scalar and fermion cross-section decreases with increasing centre-of-mass energy as s^{-1}. In the spin-1 case, however, the cross section tends to a constant in the UV.

2.1.3 Charged vector bosons are gauge bosons

The generality of (2.10) can be demonstrated already at the tree level. We start by considering the Lagrangian containing all possible terms with at most mass dimension 4 allowed by gauge symmetry,

$$\begin{aligned}\mathcal{L}_1 = {} & D^{\mu_1}V^{\nu_1}(D^{\mu_2}V^{\nu_2})^\dagger a^1_{\mu_1\nu_1\mu_2\nu_2} + m^2 V_\mu V^{\mu\dagger} \\ & + iqF^{\mu_1\nu_1}V^{\mu_2}V^{\dagger\nu_2}a^2_{\mu_1\nu_1\mu_2\nu_2} + V^{\mu_1}V^{\dagger\nu_1}V^{\mu_2}V^{\dagger\nu_2}a^3_{\mu_1\nu_1\mu_2\nu_2} \end{aligned} \tag{2.19}$$

and then, step-by-step, reduce it to (2.10). The coupling constants a^i_j can be collected into tensors describing all possible contractions between the indices

$$a^i_{\mu_1\nu_1\mu_2\nu_2} := a^i_1 g_{\mu_1\nu_1}g_{\mu_2\nu_2} + a^i_2 g_{\mu_1\mu_2}g_{\nu_1\nu_2} + a^i_3 g_{\mu_1\nu_2}g_{\nu_1\mu_2} + a^i_4 \varepsilon_{\mu_1\nu_1\mu_2\nu_2}.$$

The combinations of the vector fields the tensors $a^i_{\mu_1\nu_1\mu_2\nu_2}$ are contracted with lead to the following symmetries: $a^i_{\mu_1\nu_1\mu_2\nu_2} = a^i_{\mu_2\nu_2\mu_1\nu_1} = a^i_{\nu_1\mu_1\nu_2\mu_2}$, and thus we can impose

$$a^2_1 = a^2_3 = 0, \qquad a^3_3 = a^3_4 = 0 \tag{2.20}$$

without loss of generality. 10 parameters remain: the charge, the mass, 4 parameters in the kinetic term, 2 in the non-minimal EM interaction and 2 in the self-interaction terms. Further reduction is possible by noting that

$$\begin{aligned} D^{\mu_1}V^{\nu_1}(D^{\mu_2}V^{\nu_2})^\dagger &= \partial^{\mu_1}(V^{\nu_1}(D^{\mu_2}V^{\nu_2})^\dagger) - V^{\nu_1}D^{\mu_1}D^{\mu_2}V^{\dagger\nu_2} \\ &\sim i\frac{q}{2}V^{\nu_1}F^{\mu_1\mu_2}V^{\dagger\nu_2} - \frac{1}{2}V^{\nu_1}\{D^{\mu_1}, D^{\mu_2}\}V^{\dagger\nu_2}. \end{aligned} \tag{2.21}$$

The surface term was neglected in the last equation. It follows that a^2_i can be completely absorbed into a^1 by making the following redefinitions

$$a'^1_1 = a^1_1 + a^2_2 - a^2_3, \quad a'^1_2 = a^1_2, \quad a'^1_3 = a^1_3 - a^2_2 + a^2_3, \quad a'^1_4 = a^1_4 - 2a^2_4.$$

The kinetic term now reads

$$V^{\mu_1}(-\partial^{\nu_1}\partial^{\nu_2}a'^1_{\mu_1\nu_1\mu_2\nu_2} + m^2 g_{\mu_1\mu_2})V^{\dagger\mu_2}, \tag{2.22}$$

from which we obtain the inverse propagator in momentum space

$$i(D^{-1})_{\mu_1\mu_2} = \left(-\xi^{-1}k^2 + m^2\right)\frac{k^{\mu_1}k^{\mu_2}}{k^2} + (a_2'^1 k^2 + m^2)\left(g_{\mu_1\mu_2} - \frac{k^{\mu_1}k^{\mu_2}}{k^2}\right),$$

where we defined $-\xi^{-1} = a_1'^1 + a_2'^1 + a_3'^1$. In the propagator is

$$-iD_{\mu_1\mu_2} = \frac{-g_{\mu_1\mu_2} + k_{\mu_1}k_{\mu_2}/m^2}{k^2 - m^2} - \frac{k_{\mu_1}k_{\mu_2}/m^2}{k^2 - \xi m^2}, \tag{2.23}$$

where we fixed the overall normalisation by requiring $a_2'^1 = -1$ to obtain a pole at $k^2 = m^2$. The last term in the propagator implies a transversal degree of freedom with mass ξm^2. Its propagator has a wrong sign, making it a ghost. An identical term appears commonly through gauge fixing and is eliminated from the physical spectrum by the Faddeev–Popov ghost in non-Abelian gauge theories [78]. The field V_μ is, however, not a gauge field nor have we introduced a Faddeev–Popov ghost, which leads us to the conclusion that this transversal degree of freedom is physical. To avoid the instability accompanying degrees of freedom with a negative kinetic energy it is necessary to impose $\xi^{-1} = 0$.[1]

The propagator fixes two out of three possible parameters. The third does not contribute to the propagator as it gives a surface term, but it can still enter through the interactions. Thus, at the classical level, the general ghost free-Lagrangian of a charged vector field V_μ can be expressed as

$$\begin{aligned}\mathcal{L}_V = &-\frac{1}{2}|V^{\mu\nu}|^\dagger + m^2|V|^2 - iq((g-1)F^{\mu\nu} + \kappa\tilde{F}^{\mu\nu})V_\mu V_\nu^\dagger \\ &- \frac{\lambda_1}{2}(|V|^2)^2 + \frac{\lambda_2}{2}|V^2|^2\end{aligned} \tag{2.24}$$

where we reparametrised the Lagrangian 5 of independent physical parameters: the mass m, the gyromagnetic ratio $g \equiv a_3'^1$ and its electric equivalent $\kappa = -2a_4^2$ and two self-interaction terms $\lambda_1 = a_2^3 + a_3^3$, $\lambda_2 = -a_1^3$. $V^{\mu\nu} \equiv D^\mu V^\nu - D^\mu V^\nu$ denotes the charged vector field tensor after minimal substitution, $\tilde{F}^{\mu\nu} \equiv \epsilon^{\mu\nu\rho\sigma}F_{\rho\sigma}/2$ is the dual of $F^{\mu\nu}$. The non-minimal terms contribute to the magnetic and give rise to the electric dipole (μ,

[1] Note that this choice, as it corresponds to $\xi \to \infty$, is reminiscent of the unitary gauge.

$\tilde{\mu}$) and quadrupole (Q, $\tilde{Q}$) moments [87–89]

$$\mu = \frac{q}{2m}g, \qquad \tilde{\mu} = \frac{q}{m}\kappa \tag{2.25}$$

$$Q = -\frac{q}{2m^2}(g-1), \qquad \tilde{Q} = -\frac{q}{m^2}\kappa. \tag{2.26}$$

The Feynman rules corresponding to (2.24) are as follows: The VVA vertex is

$$iq\big((p_+ + (1-g)k)^\nu g^{\rho\mu} - (p_- + (1-g)k)^\mu g^{\rho\nu} + \\ + (p_- - p_+)^\rho g^{\nu\mu} + \kappa k_\sigma \varepsilon_{\rho\mu\sigma\nu}\big), \tag{2.27a}$$

the $VVAA$ vertex is

$$-iq^2(2g^{\mu\nu}g^{\rho_1\rho_2} - g^{\mu\rho_1}g^{\nu\rho_2} - g^{\nu\rho_1}g^{\mu\rho_2}), \tag{2.27b}$$

and the V^4 vertex is

$$-i(2\lambda_1 g^{\mu_1\mu_2}g^{\nu_1\nu_2} + \lambda_2(g^{\mu_1\nu_1}g^{\mu_2\nu_2} + g^{\mu_1\nu_2}g^{\mu_2\nu_1})). \tag{2.27c}$$

The Lorentz index μ corresponds to incoming positive charge or outgoing negative charge, the Lorentz index ν corresponds to outgoing positive charge or incoming negative charge and the Lorentz index ρ is attached to the photon. The momenta $p_\pm$, k are attached to incoming positive and negative charges and the photon, respectively.

The Lagrangian (2.24) assumed gauge invariance and the absence of ghosts of the classical theory. The requirement of perturbative unitarity additionally fixes the non-minimal terms and the self-interaction of the vector field V_μ. As can be shown by direct calculation, the unitarity of the tree level $\gamma\gamma \to VV$ scattering sets the gyromagnetic ratio to $g = 2$, $\kappa = 0$, while the unitarity of $VV \to VV$ scattering imposes $\lambda_1 = \lambda_2 = e^2$. Violation of these identities causes the mentioned cross-sections to grow as the square of the centre-of-mass energy in the UV. Fixing the parameters yields the Lagrangian (2.10) and thus the symmetry is enlarged from $U(1)$ to $SU(2)$!

The explicit mass term will still violate unitarity in VV scattering albeit more softly. However, if the masses are generated via spontaneous breaking of this enlarged symmetry the theory will be unitary and renormalisable [90]. The need for introducing scalars is a consequence of the

general result dictating that unitary and renormalisable interactions between vectors must be gauge interactions [83–85].

The minimal scenario for vectors with an $U(1)$ charge is thus reminiscent of the Georgi–Glashow model of electroweak interactions [91] where one breaks $SU(2) \to U(1)$ with an triplet scalar. However, as any compact non-abelian gauge-group contains a $SU(2)$ subgroup, the symmetry breaking pattern for $G \to U(1)$ may be more complicated. At the leading order, as long as we are interested in the interactions between V and the photons only, it is not necessary to specify the origin of the mass of V because it can cause unitarity violation only in the self-interaction of V.

2.2 Milli-charge through mixing

In case the dark sector contains its own $U'(1)$ gauge boson B'_μ, it is possible to mix B'_μ and the SM photon B_μ. Through this process the particles of the dark sector initially charged only under $U'(1)$ can obtain a small electric charge, dubbed milli-charge. There are two possible ways different $U(1)$ gauge bosons B_μ and B'_μ can mix: kinetic and mass mixing.

Reconciliation of milli-charged particles with the SM needs to account for the electroweak interactions. In extensions containing a new neutral gauge boson, which we will denote as Z', the new boson will mix with both the photon and the Z boson. Notably, milli-charged vector particles imply the existence of an additional dark $SU(2)$ gauge interaction so the SM needs to be embedded at least in a $SU(3)_c \times SU(2)_L \times SU(2)_D \times U(1)_Y$ theory.

2.2.1 Kinetic mixing

Kinetic mixing happens if the kinetic term is non-diagonal,

$$\frac{1}{4}\left(B^{\mu\nu}B_{\mu\nu} + B'^{\mu\nu}B'_{\mu\nu} - 2\chi B'^{\mu\nu}B_{\mu\nu}\right), \tag{2.28}$$

where χ is a constant and $B_{\mu\nu}$ and $B'_{\mu\nu}$ are the field tensors of B_μ and B'_μ, respectively. A fundamental kinetic mixing term is allowed by gauge symmetries, unitarity and renormalisability and, even if it set to zero a tree level, it arises naturally through radiative corrections if the theory contains

heavy fermions charged under both gauge groups [56]. The kinetic term (2.28) can be canonically normalised by defining the new states

$$A'_\mu = B'_\mu - \chi B_\mu, \qquad A_\mu = \sqrt{1-\chi^2} B_\mu. \tag{2.29}$$

The vectors A_μ and A'_μ represent the propagating eigenstate of the photon and the dark photon, respectively.

To see how the dark sector particles could obtain a milli-charge, notice that a field carrying a dark charge q_D but not an electric charge is, by definition, acted upon by the covariant derivative $D_\mu = \partial_\mu + iq_D B'_\mu$. In terms of the redefined fields (2.29) this becomes $D_\mu = \partial_\mu + iq_D A'_\mu + iq\, eA_\mu$, where

$$q = -\frac{q_D}{e}\frac{\chi}{\sqrt{1-\chi^2}} \tag{2.30}$$

is the electric charge of a particle with a non-vanishing dark charge q_D. On the other hand, electrically charged particles will not acquire a dark charge, because the photon field is just rescaled (the rescaling will enter the fine structure constant, though). This asymmetry is a result of the non-orthonormality of the transformation (2.29).

2.2.2 Mass mixing

The field redefinition that diagonalises the kinetic term (2.28) is not unique. As A_μ and A'_μ are canonically normalised, any orthogonal transformation would give a new set of canonically normalised fields. This freedom was implicitly used above to choose a basis in which electrically charged particles do not obtain a dark charge. This would not be possible if the fields are massive, because the mass eigenstates fix a preferred basis for propagation and the SM electromagnetic interaction would then comprise two different forces distinguishable by their range. Moreover, if the vector fields masses are non-degenerate, then a non-diagonal mass term will mix the fields even if their kinetic term is diagonal. This captures the essence of the second way of generating mixtures of gauge bosons.

The Stückelberg extension of the SM

The minimal model for mass mixing is the Stückelberg extension of the SM [92, 93]. It appends a dark $U(1)_D$ gauge group to the electroweak

$U(1)_Y \times SU(2)_L$ and breaks it to the electromagnetic $U(1)_{EM}$ by the SM Higgs ϕ and an additional dark scalar singlet ϕ_D carrying both the hypercharge and a dark $U(1)_D$ charge. The covariant derivative (neglecting $SU(3)$ interactions) reads

$$D_\mu = \partial_\mu - ig_1 B_\mu Y - ig_2 W_\mu^i \tau_i - ig_D B'^i_\mu Q_D \tag{2.31}$$

where τ_i are the generators of $SU(2)_L$, Y denotes the hypercharge, and Q_D denotes the dark charge. g_1, g_2 and g_D are the coupling constants of the SM and the dark sector, respectively.

The charge corresponding to the residual symmetry $U(1)_{\mathrm{EM}}$, i.e. the electric charge, is given by a generalised Gell-Mann–Nishijima formula

$$Q = I_3 + Y + \epsilon Q_D, \tag{2.32}$$

where $\epsilon \equiv -Y_{\phi_D}/Q_{D,\phi_D}$ is the milli-charge, Y_{ϕ_D}, Q_{D,ϕ_D} are the hypercharge and the dark charge of ϕ_D, respectively. The charge is expressed in units of the elementary charge

$$e = (g_1^{-2}(1+\xi^2) + g_2^{-2})^{-1/2}, \tag{2.33}$$

where we defined the quantity $\xi \equiv \epsilon g_D/g_1$ that quantifies the strength of mixing of the dark and visible neutral bosons. Any particle with a dark charge Q_D will therefore also carry an electric charge ϵQ_D. This is due to mass mixing. Decoupling from the SM corresponds to $\xi = 0$, $\epsilon = 0$. In the following we assume that the deviation form the SM is small, i.e. $\epsilon, \xi \ll 1$, which we will refer to as the weak coupling limit. The smallness of ϵ implies that the hypercharge of ϕ_D must also be small.

The neutral gauge boson mass matrix generated by spontaneous symmetry breaking reads in the basis $E^T = (B', B, W_3)$ [76, 92]

$$M^2 = \begin{pmatrix} m^2_{Z'_0} & -m^2_{Z'_0}\xi & 0 \\ -m^2_{Z'_0}\xi & s^2_W m^2_{Z_0} + m^2_{Z'_0}\xi^2 & -m^2_{Z_0} c_W s_W \\ 0 & -m^2_{Z_0} c_W s_W & m^2_{Z_0} c^2_W \end{pmatrix}, \tag{2.34}$$

where c_W, s_W denote the cosine and sine of the Weinberg angle θ_W, respectively. The mass matrix has a zero eigenvalue corresponding to the photon and two non-vanishing eigenvalues corresponding to the tree level

Z and Z' bosons masses, respectively. At leading order in ξ the masses read

$$m_Z^2 = m_{Z_0}^2 + \xi^2 m_{Z'_0}^2 \frac{m_{Z_0}^2 s_W^2}{m_{Z_0}^2 - m_{Z'_0}^2} + \mathcal{O}(\xi^4), \tag{2.35}$$

$$m_{Z'}^2 = m_{Z'_0}^2 + \xi^2 m_{Z'_0}^2 \left(1 - \frac{m_{Z_0}^2 s_W^2}{m_{Z_0}^2 - m_{Z'_0}^2}\right) + \mathcal{O}(\xi^4), \tag{2.36}$$

where the subindex 0 denotes the corresponding fields in the decoupling limit. In the weak coupling limit, the mass eigenstates are naturally expressed through two consecutive rotations. Exact decoupling corresponds to the eigenstates

$$\begin{pmatrix} Z'_0 \\ A_0 \\ Z_0 \end{pmatrix} = \begin{pmatrix} 1 & 0 & 0 \\ 0 & c_W & s_W \\ 0 & -s_W & c_W \end{pmatrix} \begin{pmatrix} V_3 \\ B \\ W_3 \end{pmatrix}, \tag{2.37}$$

and the eigenstates in a coupled theory are obtained by the rotation

$$\begin{pmatrix} Z' \\ A \\ Z \end{pmatrix} = \begin{pmatrix} c_1 c_2 & -s_1 c_2 & -s_2 \\ s_1 & c_1 & 0 \\ c_1 s_2 & -s_1 s_2 & c_2 \end{pmatrix} \begin{pmatrix} Z'_0 \\ A_0 \\ Z_0 \end{pmatrix}, \tag{2.38}$$

where $c_{1,2}$ and $s_{1,2}$ are the cosines and sines of the additional mixing angles θ_1 and θ_2 that in the weak coupling limit are given by

$$\theta_1 \approx -\xi c_W, \qquad \theta_2 \approx -\xi \frac{m_{Z'_0}^2 s_W}{m_{Z'_0}^2 - m_{Z_0}^2}. \tag{2.39}$$

The expansion coefficient in Eq. (2.39) implies that in addition to $\xi \ll 1$ it is necessary to assume that the neutral boson masses are degenerate, $m_{Z'_0} \neq m_{Z_0}$, and that the Z' should not be significantly heavier than the Z. The leading order expressions for the masses and the mass eigenstates can be obtained easily via diagrammatic methods by treating the ξ dependent terms in (2.35) as interaction terms corresponding to two-legged vertices.

Although the original Stückelberg extension [92] does not involve kinetic mixing nor any other particles and thus no candidates for milli-charged particles, it is relatively straightforward to include these [94, 95].

Milli-charged vector bosons

As shown in Sec. 2.1 milli-charged scalars and fermions (spin 1/2) can be constructed by minimal substitution. Inclusion of milli-charged vector particles, however, necessitates an extension of the underlying gauge group. Minimally, instead of appending a dark $U(1)_D$ to the SM gauge group we must include a $SU(2)_D$ [76]. The covariant derivative (neglecting strong interactions) now reads

$$D_\mu = \partial_\mu - ig_1 B_\mu Y - ig_2 W^i_\mu \tau_i - ig_D V^i_\mu \tau_{D,i} \tag{2.40}$$

where $\tau_{D,i}$ are the generators of $SU(2)_D$. Analogously to the SM, after the symmetry braking the dark sector can be described by one neutral V_3 and two complex vector fields $V_\pm = (V_1 \pm iV_2)/\sqrt{2}$.

The $SU(2)_D \times U(1)_Y$ is broken to $U(1)_{EM}$ by the dark scalar ϕ_D. The two groups will mix only if the scalar carries a hypercharge. In that case, the fact that the group is not completely broken implies that the vacuum state of ϕ_D is an eigenstate of an $SU(2)_D$ generator, which we can choose to be $\tau_{D,3}$ without loss of generality. The residual $U(1)_{EM}$ will be automatic for a ϕ_D in the fundamental or adjoint representation of $SU(2)_D$, but needs to be additionally assumed for larger representations.

The tree-level masses in the decoupling limit are given by

$$m_W = \frac{v g_2}{2}, \qquad m_{Z_0} = \frac{m_W}{c_W}, \tag{2.41}$$

$$m_V = v_D g_D |I_{D3,0}| r, \qquad m_{Z'_0} = \frac{m_V}{r}, \tag{2.42}$$

where $v_D \equiv |\phi_D|$ denotes the vacuum expectation value of the dark scalar. We defined the parameter

$$r \equiv \sqrt{(I_{D,0}(I_{D,0}+1) - I^2_{D3,0})/(2I^2_{D3,0})}, \tag{2.43}$$

where $I_{D3,0}$ denotes the dark isospin, i.e. eigenvalue of the τ_{D3}, of ϕ_D. The minimal choice, a dark scalar doublet ϕ_D, gives $r = 1$ and therefore $m_{Z'_0} = m_V$. The mass matrix of the neutral gauge bosons is identical to the mass matrix (2.34) of the Stückelberg Z' model. However, the (milli)charge appears now in discrete units. The generalised Gell-Mann–Nishijima formula Eq. (2.32) reads

$$Q = I_3 + Y + \epsilon I_{D3}, \tag{2.44}$$

The dark isospin of the vector fields $V_\pm$ is $I_{D3} = \pm 1$, so they will carry a milli-charge $\pm\epsilon$.

3 Can dark matter be charged?

The nature of DM beyond its gravitational interactions is one of the outstanding problems of contemporary physics. In the standard cosmological model DM is assumed to be cold and inert.

3.1 Experimental status of cold dark matter

The existence of DM was first suggested in 1933 by Fritz Zwicky's study of the Coma Cluster [96]. He analysed the velocity dispersion of the galaxies within the cluster and came to the conclusion that the mass of the cluster should be much larger than implied by the luminous matter. He coined the term "dunkle Materie" to denote the non-luminous component. Later in the same decade it was noticed that the stars of the outer parts of the galactic disk of the Andromeda galaxy moved faster than expected [97]. This was confirmed several decades later [98, 99]. It was observed that the velocities of the stars were roughly constant at large distances from the centre of the galaxy while the distribution of luminous matter implied that the velocities should decrease with the distance. The rotation curves of spiral galaxies became the first widely accepted evidence for the existence of DM.

Mass estimates of galaxy clusters indicate that they only contain approximately one sixth of baryonic matter. As they are the largest gravitationally bound objects of the universe it is expected that this fraction should roughly represent the average in the entire visible Universe. The total mass of the cluster can be estimated in several ways. If light from more distant sources passes the cluster its path will be bent depending on the strength of gravitational field of the cluster. This effect causes the phenomenon of gravitational lensing [100, 101] and can provide useful information about not only the total mass but also about the substructure of the cluster. Dynamical estimates of the cluster mass are obtained e.g.

Figure 3.1: An image of the Bullet Cluster combining the stars, the X-ray luminous gas [104] (in red) and the DM distribution inferred from weak lensing [105] (in blue).

from the velocity dispersion of galaxies [96] or the temperature profile of X-ray emitting gas if it is in hydrostatic equilibrium [102].

A remarkable piece of evidence for DM comes from astrophysical observations of galaxy cluster collisions. The best known example of these rare events is probably galaxy cluster 1E 0657-56, known as the Bullet Cluster. It was discovered in 1995 [103] and first observed by the Chandra X-ray observatory. The substructure of the the Bullet Cluster, show in Fig. 3.1, reveals that it was formed by the collision of two clusters with masses roughly ten times different. The smaller cluster, the "bullet", moved through the larger one at roughly 4700 km/s. While the stars moved almost freely, the intracluster gas interacted and left behind a prominent bow shock composed of hot X-ray emitting gas [5–7]. Comparison of the weak lensing analysis reveals a dark clump on top of the stars that is separated from the gas and the larger cluster implying that the dark matter component had passed through similarly to the stars. This observation supports the hypothesis that DM is a collisionless gas of particles.

The measurements of the CMB anisotropy and the large scale structure of the Universe provide perhaps the most compelling evidence for a non-baryonic matter component. The most precise determination of the DM abundance is inferred from the observation of the angular power spectrum of CMB anisotropies by the Planck satellite. In the ΛCDM model the energy density of the baryonic matter and CDM is respectively [106]

$$\Omega_b h^2 = 0.02226(23), \qquad \Omega_c h^2 = 0.1186(20). \tag{3.1}$$

The ratio of these quantities is consistent with the estimate from galaxy clusters. The energy density is expressed in terms of the density parameter $\Omega_i \equiv \rho_i/\rho_{\rm crit}$, where $\rho_{\rm crit} \equiv 3M_{\rm Pl}^2 H_0^2$ is the critical density, $M_{\rm Pl} = (8\pi G)^{-1/2}$ is the reduced Planck mass and $H_0 \equiv h \times 100\,{\rm km\,s^{-1}\,Mpc^{-1}}$ is the Hubble constant. The value of the Hubble constant inferred from the Planck satellite data is $h = 0.6727(66)$ [106] which, assuming the ΛCDM model, is in 3σ tension with the estimate from Type Ia supernovae which implies $h = 0.738(24)$ [107–111].

Despite the successes of the ΛCDM model, cosmological N-body simulations fail to predict some of the observed features at small scales, that is, at scales smaller than the size of typical galaxies (for a review see Refs. [22, 112]).

Numerical simulations show that hierarchical structure formation in ΛCDM produces self-similar DM haloes well described by the Navarro–Frenk–White profile [113]

$$\rho(r) = \frac{\rho_0}{r/r_s(1 + r/r_s)}, \tag{3.2}$$

where ρ_0 is a density scale and r_s is the scale radius. These haloes have sharply peaked central densities, yet the observed galactic rotation curves indicate that the central region is less massive than for the cuspy profiles found in the simulations. So density profiles with a constant density core are favoured. This discrepancy is dubbed the core-cusp problem [17, 18]. An additional issue is the simplicity of the NFW profile – its shape is determined by a single parameter implying that there is a high degree of correlation between other possible characteristics of the halo shape. This is at odds with the diversity of the observed rotation curves [114].

The CDM haloes produced in N-body simulations have a rich substructure. The number of subhaloes predicted by simulations mostly exceeds

the number of observed Milky Way satellites by at least one order of magnitude [15, 16]. This is called the missing-satellites problem. However, the small number of observed low-mass satellites could be explained by some not so well understood baryonic effect that, for example, causes them to be much fainter. The heaviest and most luminous Milky Way subhaloes are subject to the too-big-to-fail problem – these subhaloes seem to be several times lighter than the CDM based simulations predict [19, 20].

It is too early to tell whether these conflicts are solved by modifying the ΛCDM model or by improving our knowledge of galaxy formation. The small-scale problems generally seem to require suppression of the small scale power spectrum. A possible solution is, for example, provided by fuzzy dark matter, an extremely light scalar field that can not form clumps smaller than its de Broglie wavelength which can be of the size of a dwarf galaxy [115]. A less exotic resolution to the small-scale problems is offered by DM self-interactions [21, 22].

Cluster collisions provide an invaluable testing ground for DM self-interactions (for a review see Ref. [22]). The Bullet Cluster is consistent with the collisionless DM paradigm and implies an upper bound for the DM self-interaction cross section of $\sigma/m \lesssim 0.7\text{cm}^2/\text{g}$. On the other hand, the explanation of the Abell 3827 and Abell 520 clusters by an interacting DM scenario requires $\sigma/m \gtrsim 1.5\text{cm}^2/\text{g}$ [116] and $\sigma/m \gtrsim 1\text{cm}^2/\text{g}$ [24, 117], respectively. The Bullet Cluster constraint is, however, obtained by assuming that all DM is self-interacting and can thus be relaxed in scenarios where only a subcomponent of DM is interacting. This situation has been studied in the context of the Abell 520 cluster [27, 28].

3.2 Thermal history of (dark) matter

The early universe is filled with a heat bath of relativistic particles. All particles of the SM are expected to be in thermal equilibrium at temperatures above 1 MeV. Kinetic equilibrium is reached through elastic scattering, and chemical equilibrium is established by processes that can create and destroy particles, such as annihilation or pair creation. Depending on the strength of the relevant interactions, the dark sector may or may not reach equilibrium with itself or with the SM.

CMB observations indicate that the early Universe was homogeneous,

isotropic and spatially flat to a very high degree [2]. The corresponding spacetime geometry is thus well modelled by a Friedmann–Robertson–Walker spacetime with the metric tensor

$$g_{\mu\nu} = \mathrm{diag}(-1, a^2\delta_{ij}), \tag{3.3}$$

where a denotes the scale factor. The expansion history, that is, the evolution of the Hubble parameter, $H \equiv \dot{a}/a$, follows from the Friedmann equation

$$H^2 = \frac{1}{3M_{\mathrm{Pl}}^2} \sum_i \rho_i \tag{3.4}$$

where $M_{\mathrm{Pl}} = (8\pi G)^{-1/2}$ is the reduced Planck mass and ρ_i is the energy density of the i-th component. It is customary to introduce the density parameters $\Omega_i \equiv \rho_i/\rho_c$, where $\rho_c \equiv 3M_{\mathrm{Pl}}^2 H^2$ is the critical density. In the following Ω_i will denote the present density parameters.

3.2.1 Effective numbers of degrees of freedom

The phase space density of a particle species in thermal equilibrium follows a Bose–Einstein or a Fermi–Dirac distribution,

$$f(\mathbf{p}) = \frac{g_i}{e^{(E(\mathbf{p})-\mu)/T} + \eta}, \tag{3.5}$$

depending on wether the particle is a fermion ($\eta = +1$) or a boson ($\eta = -1$). Here μ denotes the chemical potential, T is the temperature, $\mathbf{p}$ the three-momentum and g_i stands for the internal degrees of freedom of the species. Maxwell–Boltzmann statistics ($\eta = 0$) is a good approximation when $T \ll \mu$ or $T \ll m$, since in this case the contribution of η can be ignored. The energy density is given by

$$\rho_i \equiv \int \frac{\mathrm{d}^3\mathbf{p}}{(2\pi)^3} f(\mathbf{p})\, E(\mathbf{p}) \tag{3.6}$$

and other thermodynamic observables, such as pressure, entropy density and number density, can be evaluated analogously. For ultrarelativistic species ($T \gg m$)

$$\rho_i = \begin{cases} (7/8)(\pi^2/30)\, g_i T^4, & \eta = +1 \text{ (Fermi)}, \\ (\pi^2/30)\, g_i T^4 & \eta = -1 \text{ (Bose)}. \end{cases} \tag{3.7}$$

Based on the analogy with the above formula one defines the effective number of (bosonic) relativistic degrees of freedom $g_*(T)$ at temperature T by

$$\rho(T) \equiv \frac{\pi^2}{30}\, g_*(T)\, T^4. \tag{3.8}$$

In a radiation dominated Universe the number of degrees of relativistic freedom is estimated by

$$g_*(T) \approx \sum_{i \in \text{bosons}} g_i \left(\frac{T_i}{T}\right)^4 + \frac{7}{8} \sum_{i \in \text{fermions}} g_i \left(\frac{T_i}{T}\right)^4, \tag{3.9}$$

where the sums run over relativistic species and T_i denotes the temperature of the species i. The temperature T is usually taken to match the temperature of the photons. At temperatures $T > m_t = 173\,\text{GeV}$ all degrees of freedom of the SM contribute giving $g_* = 106.75$. The number of bosonic degrees of freedom comprises gluons ($8 \times 2 = 16$), photons (2), W and Z bosons ($3 \times 3 = 9$) and Higgs (1), and the fermionic one consists of quarks ($3 \times 3 \times 4 = 36$), charged leptons ($3 \times 4 = 12$), and neutrinos ($3 \times 2 = 6$). The SM degrees of freedom are in thermal equilibrium until the decoupling of neutrinos at $T \approx 1\,\text{MeV}$ and thus before $T_i = T$ for all particles of the SM. The dark sector can contain particles thermally decoupled from the SM which will thus generally have a temperature different from the photons.

The evolution of temperature can be derived by using the fact that the entropy in a comoving volume is conserved for adiabatic processes. The entropy density s will thus scale as a^{-3}. In a thermal bath of relativistic particles the total entropy density can be expressed as

$$s(T) = \frac{2\pi^2}{45}\, g_{*s}(T)\, T^3, \tag{3.10}$$

where $g_{*s}(T)$ is also called the number of relativistic degrees of freedom. It can approximated by [118]

$$g_{*s}(T) \approx \sum_{i \in bosons} g_i \left(\frac{T_i}{T}\right)^3 + \frac{7}{8} \sum_{i \in fermions} g_i \left(\frac{T_i}{T}\right)^3. \tag{3.11}$$

If $T_i = T$, then $g_{*s} = g_*$. Conservation of comoving entropy now implies that

$$T \propto a^{-1} g_{*s}^{-1/3}. \tag{3.12}$$

This holds for species that are kinetically coupled. Note that $H \propto T^2 \propto \dot{T}/T$ implying $t \propto T^{-2}$.

A decoupled relativistic particle will retain the shape of its thermal distribution and thus it makes sense to talk about it's temperature even if the particle is inert. The evolution of the temperature of this particle can be estimated by noting that the momentum scales as a^{-1}. Plugging this scaling into the phase space distribution which for thermal ultra-relativistic particles depends on the temperature only through the ratio $|\mathbf{p}|/T$, we see that the temperature must scale as $T \propto a^{-1}$. The distribution of a decoupled non-relativistic particle depends on the temperature through the combination $|\mathbf{p}|^2/T$, and therefore $T \propto a^{-2}$.

Assuming only the SM particle content, at $T > 1$MeV all the SM degrees of freedom are in thermal equilibrium and thus $g_{*,\mathrm{SM}} = g_{*s,\mathrm{SM}}$. However, the neutrinos decouple shortly after. So, when electrons and positrons dump their entropy to the thermal bath when the temperature drops below $T \approx 0.5$MeV only the temperature of photons grows. The entropy of the neutrinos and of the rest of the visible sector are conserved separately implying

$$\left.\frac{g_{s*,\gamma}(T_\gamma) T_\gamma^3}{g_{s*,\nu}(T_\nu) T_\nu^3}\right|_t = const., \tag{3.13}$$

where $g_{s*,\gamma}$, $g_{s*,\nu}$ are the effective relativistic degrees of freedom coupled to photons and neutrinos, respectively. The increase of the temperature of the photons follows from the fact that the number of relativistic degrees of freedom coupled to photons, $g_{s*,\gamma}$, drops from 5.5 to 2 after the electrons and positrons freeze out, so $T/T_\nu = (11/4)^{1/3}$. It follows that $g_{*s,SM}(T_0) = 3.94$, so the present SM entropy density is $s_0 \approx 2900\,\mathrm{cm}^{-3}$, where we used the present CMB temperature $T_0 = 2.7260 \pm 0.0013$K [119].

Big bang nucleosynthesis (BBN) takes place at temperature about $T \approx 1$MeV, comparable to the temperature of neutrino decoupling [118]. The relic abundance of nuclei is very sensitive to the expansion of the universe and thus also to the abundance of dark radiation at that time. Therefore,

the observed ratio of light nuclei implies an upper bound on the number of hidden degrees of freedom lighter than 1MeV that are thermalised with the visible sector [120]. The CMB is also sensitive to the radiation content of the Universe at recombination. The energy density of dark radiation in the late early Universe is commonly parametrised by the effective number of neutrinos $N_{\rm eff}$ that can be defined by

$$g_*(T) \equiv 2 + 2 \times \frac{7}{8} N_{\rm eff} \left(\frac{4}{11}\right)^{4/3} \tag{3.14}$$

at temperatures below neutrino decoupling. In the SM $N_{\rm eff,SM} = 3.046$, because the neutrinos do not completely decouple before electrons and positrons annihilate and thus they are slightly heated [121]. This prediction is in very good agreemFent with the value $N_{\rm eff} = 3.15 \pm 0.23$ inferred from CMB observations by the Planck sattellite [2]. However, an $N_{\rm eff}$ slightly larger than the SM prediction might be favored [122] as it could relieve the tension between the low and high redshifts measurements of σ_8 and the Hubble constant H_0 [108–111].

The temperature of the dark and visible sectors may be different. To quantify this difference we define the ratio

$$\zeta(T) \equiv \frac{T_{\rm D}}{T}. \tag{3.15}$$

Entropy conservation implies that the ratios at different temperatures, T and T_*, are related by

$$\zeta(T) = \left(\frac{g_{s*,\gamma}(T)}{g_{s*,\gamma}(T_*)} \frac{g_{s*,D}(T_*\zeta(T_*))}{g_{s*,D}(T\zeta(T))}\right)^{1/3} \zeta(T_*). \tag{3.16}$$

If the two sectors were in kinetic equilibrium at some high temperature then it is convenient to choose T_* at the temperature where the two sectors decouple, in that case $\zeta(T_*) = 1$. From (3.9) we find that the effective number of neutrinos at $T \ll 1$MeV is

$$N_{\rm eff} = N_{\rm eff,SM} + \frac{11}{7}\left(\frac{11}{4}\right)^{1/3} \zeta(T)^{4/3} g_{*,D}(T). \tag{3.17}$$

The measured value $N_{\rm eff} = 3.15 \pm 0.23$ corresponds to $\zeta^{4/3} g_{*,D} \leq 0.15$ at 1σ confidence level. The existence of a massless dark photon, $g_{*,D}(T_{\rm CMB}) \geq 2$,

is therefore allowed at the 2σ confidence level if $\zeta(T_{\rm CMB}) \leq 0.21$, that is, when the dark photons are more than four times colder than the visible sector.

A similar bound can be obtained from BBN [74] as the ratios of light nuclei imply $N_{\rm eff} = 3.24 \pm 1.2$ at 2σ confidence level [123]. Although the resulting constraint is weaker, it applies to light degrees of freedom with masses up to 1MeV.

3.2.2 The Boltzmann equation

Consider the production of DM from a thermal bath of SM particles. We will mainly focus the discussion to the scenario where DM is produced through a DM DM $\leftrightarrow N \times$ SM interaction, that is, DM pair production from and annihilation to the visible sector. Other common channels, which are not considered here, are DM decay/inverse decay and coannihilation.

The distribution of any particle species evolves according to the Boltzmann equation [118]

$$\mathbf{L}[f] = \mathbf{C}[f], \tag{3.18}$$

where $\mathbf{C}$ the collision operator accounting for particle interactions and $\mathbf{L}$ denotes the Liouville operator describing the motion of free-streaming particles along geodesics.

Integration of the Boltzmann equation (3.18) over the phase space yields an equation for the evolution of the number density n of a species of particles, which is also called the Boltzmann equation,

$$\partial_t n + 3Hn \equiv -\langle \sigma \, v_{\rm M\o l} \rangle \left(n^2 - n_{eq}^2 \right), \tag{3.19}$$

where σ is the annihilation cross-section for DM annihilation, $v_{\rm M\o l}$ is the Møller velocity[1] and $n_{\rm eq}$ is the equilibrium number density. The cross section σ corresponds to annihilation of the DM particles, DM DM $\to$ SM SM. The inverse process, SM SM $\to$ DM DM, is given by the n_{eq}^2 term. This can be shown by direct computation of the thermal average for this process. A simpler way to see it, however, is to use the principle of detailed balance that dictates that the left hand side of Eq. (3.19) must be zero at $n = n_{\,eq}$. By using Eq. (3.19) we ignore Bose enhancement and/or Dirac

[1] $v_{\rm M\o l} = \beta s/(2E_1E_2)$. If $m_1 = m_2 \equiv m$, then $\beta = \sqrt{1 - 4m^2/s}$ is the velocity in the c.m. frame. Moreover, in the c.m. frame $v_{\rm M\o l} = 2\beta \equiv v_{\rm rel}$.

suppression. They are negligible at low temperatures, $T \ll m$, and may introduce at most an $\mathcal{O}(1)$ correction at higher temperatures.

If the particles are free, $\langle \sigma v_{M\o l} \rangle = 0$, the comoving number density is conserved and thus $n \propto a^{-3}$. Eliminating this scaling behaviour simplifies the equations and, to this purpose, it is customary to normalise the number density with the entropy by defining the quantity

$$Y \equiv n/s. \tag{3.20}$$

So, $Y = const.$ implies that the comoving particle density is conserved because also $s \propto a^{-3}$. The current energy density of the species is $\rho = m s_0 Y_0$, where $s_0 \approx 2900\mathrm{cm}^{-3}$ is the present entropy density. Therefore

$$\Omega h^2 = 2.8 \times 10^8 \frac{m}{\mathrm{GeV}} Y_0, \tag{3.21}$$

where h is the Hubble parameter in units of $100\mathrm{km\,s^{-1}Mpc^{-1}}$. This quantity should be compared with the present CDM abundance $\Omega_c h^2 = 0.12$.

The Boltzmann equation (3.19) can be simplified further by using the dimensionless inverse temperature, $x \equiv m/T$, as the time variable, so[2]

$$\frac{\mathrm{d}Y}{\mathrm{d}x} = -\lambda \left(Y^2 - Y_{eq}^2 \right), \tag{3.22}$$

where

$$\lambda = \sqrt{\frac{8\pi^2}{45}} \frac{g_{*s}}{g_*^{1/2}} \left(1 - \frac{1}{3} \frac{\mathrm{d} \ln g_{*s}}{\mathrm{d} \ln x} \right) m M_{\mathrm{Pl}} \langle \sigma \, v_{\mathrm{M\o l}} \rangle \, x^{-2}. \tag{3.23}$$

In the numerical calculations we have omitted the derivative term in the round brackets.

[2]From the identity $\mathrm{d}n/\mathrm{d}t = aH\mathrm{d}n/\mathrm{d}a$ and entropy conservation $s \propto a^{-3}$, which implies $\mathrm{d}s/\mathrm{d}a = -3s/a$, we obtain

$$s \frac{\mathrm{d}n/s}{\mathrm{d}t} = aHs \frac{\mathrm{d}x}{\mathrm{d}a} \frac{\mathrm{d}Y}{\mathrm{d}x} = -3Hs^2 \left(\frac{\mathrm{d}s}{\mathrm{d}x} \right)^{-1} \frac{\mathrm{d}Y}{\mathrm{d}x}.$$

Equilibrium density

The number density corresponds to the following integral over the phase space

$$n \equiv \int \frac{\mathrm{d}^3\mathbf{p}}{(2\pi)^3} f(\mathbf{p}) \tag{3.24}$$

where, depending on the type of particle, in equilibrium $f(\mathbf{p})$ is either a Bose–Einstein or Fermi–Dirac distribution (3.5). Therefore

$$Y_{eq} \equiv \frac{n_{eq}}{s} = \frac{g}{g_{*s}} \frac{45}{4\pi^4}\, x^3 \int_1^\infty \frac{\sqrt{y^2-1}y\mathrm{d}y}{e^{xy}+\eta} \tag{3.25}$$

where g is the number of degrees of freedom of the particle under consideration. If $T \ll m$, or equivalently $x \gg 1$, we can use a Maxwell–Boltzmann distribution for which

$$Y_{eq} \approx 0.145 \frac{g}{g_{*s}} x^{3/2} e^{-x}. \tag{3.26}$$

The equilibrium density at higher temperatures can be approximated by truncating the series

$$Y_{eq} \approx \frac{45}{4\pi^4} \frac{g}{g_{*s}} x^2 \sum_{n>0} \frac{\eta^{n+1}}{n} K_2(nx). \tag{3.27}$$

At low temperatures, when $x \gg 1$, the higher terms in the sum are suppressed and only the first term, corresponding to the Maxwell–Boltzmann distribution, contributes. For $x > 3$ eq. (3.26) is already a decent approximation.

For high temperatures, $x \ll 1$, the equilibrium density acquires a factor $\zeta(3) \approx 1.2$ for bosons and $\zeta(3)\, 3/4 \approx 0.9$ for fermions and the limiting case reads

$$Y_{eq} \approx \frac{45\zeta(3)}{2\pi^4} \frac{g}{g_{*s}} \chi, \tag{3.28}$$

where $\chi = 1$ for bosons and $3/4$ for fermions, respectively. In the limit $x \ll 1$ the series (3.27) converges relatively slowly – as slowly as the series representation of the zeta function.

Thermal average of the cross section

Assuming a Maxwell–Boltzmann distribution, the thermal average of the cross section is [124]

$$\langle \sigma\, v_{\text{Møl}} \rangle = \frac{4x}{K_2(x)^2} \int_1^\infty \sigma(4m^2 y)\sqrt{y}(y-1)K_1(2x\sqrt{y})\,\mathrm{d}y, \tag{3.29}$$

where $s = 4m^2 y$ is the squared centre-of-mass energy of the collision. Close to the threshold $s = 4m^2$ the cross-section can be expanded in $\beta = \sqrt{1 - y^{-2}}$,

$$\sigma = \sum_{i \geq 0} \sigma_i \beta^{2i-1}. \tag{3.30}$$

Here we consider all terms that grow at most as β^{-1} when $\beta \to 0$. Unitarity forbids terms that grow faster than β^{-2} [125]. Non-resonant Sommerfeld enhancement can boost the low temperature cross section by a factor of β^{-1} [126] possibly saturating the unitarity bound. The resonant Sommerfeld enhancement allows for even faster growing boost rates [127] before the unitarity bound is reached. However, we neglect these non-perturbative effects as become relevant at too low temperatures to have a significant effect on the relic abundance [127].

The low temperature ($x \gg 1$) expansion of the thermal average (3.29) reads

$$\begin{aligned} \langle \sigma\, v_{\text{Møl}} \rangle = 2\sigma_0 &+ \left(-\frac{3}{2}\sigma_0 + 3\sigma_1 \right) x^{-1} \\ &+ \left(\frac{93}{16}\sigma_0 - \frac{9}{4}\sigma_1 + \frac{15}{2}\sigma_2 \right) x^{-2} + \mathcal{O}(x^{-3}). \end{aligned} \tag{3.31}$$

At high temperatures, $x \ll 1$, we can expand the cross section as

$$\sigma = \sum_{i \geq 0} \bar{\sigma}_i \left(\frac{4m^2}{s} \right)^i, \tag{3.32}$$

where we neglected possible logarithmic terms. Terms growing polynomially with s are forbidden by unitarity [128, 129]. The thermal average (3.29) can then be expanded as

$$\langle \sigma\, v_{\text{Møl}} \rangle = \sigma_0 + \frac{1}{2}\sigma_1 x^2 + \mathcal{O}(x^2). \tag{3.33}$$

Note that by using (3.29) we implicitly assumed Maxwell–Boltzmann statistics at high temperatures, which induces an $\mathcal{O}(1)$ error in the approximation (3.33).

3.2.3 Freeze-out

The most prominent DM production mechanism is likely the thermal freeze-out. Notably, if interactions between the SM and DM particles have cross-sections of the size typical to the weak interaction, the observed DM relic abundance is produced by freeze-out. This coincidence is known as the WIMP miracle and it has been used as a motivation for the DM candidates such as the neutralino predicted in supersymmetric extensions of the SM [10].

The freeze-out can be qualitatively understood as follows. The geometric expansion of space-time cools the primordial heat bath. If the temperature of the heat bath drops below the mass of a particle, its equilibrium number density (3.26) will drop exponentially with the temperature. As the universe cools further, at some point the number density fails to follow the rapid decline of its equilibrium value. This point is quantified by the freeze-out temperature x_{fo} that can be roughly determined by comparing the annihilation rate $\langle \sigma\, v_{\mathrm{M\o l}} \rangle n$ with the expansion rate H. At that time $n \approx n_{\mathrm{eq}}$ still holds and so the exponential dependence on the temperature implies that the freeze-out temperature depends only logarithmically on the interaction cross section. At $x > x_{\mathrm{fo}}$ the pair production of DM particles has stopped but its inverse process, the annihilation of DM particles, continues. It also stops after a while because the number density becomes more and more diluted. The evolution of the abundance with the temperature is depicted in Fig. 3.2. The stronger the interaction, the longer the annihilation lasts. As a consequence the resulting DM abundance will be inversely proportional to the interaction cross section.

To sketch the approximate solution of the Boltzmann equation (3.22) we first recast (3.22) as

$$y' = -y \ln(Y_{eq})' - \lambda Y_{eq}(y^2 - 1), \tag{3.34}$$

where $y = Y/Y_{eq}$. Using this formulation it is easier to see the departure from equilibrium, $y = 1$, by noting that the second term forces equilibrium whereas the first tries to move the system out of equilibrium. Deviations

from $y = 1$ are possible if $\ln(Y_{eq})' > \lambda Y_{eq}$. The point at which y leaves the equilibrium can be characterised by $(Y_{eq}^{-1})' = \lambda\,\delta$, where $\delta = \mathcal{O}(10)$. A good choice is $\delta \approx 8$. This condition defines the freeze-out temperature $x_{\rm fo}$. At temperatures $x > x_{\rm fo}$ the equilibrium density can be ignored and the Boltzmann equation (3.22) is well approximated by

$$\frac{\mathrm{d}Y}{\mathrm{d}x} \approx -\lambda Y^2. \tag{3.35}$$

Integrating this equation yields

$$Y(x) = \left(Y^{-1}(x_{\rm fo}) + \int_{x_{\rm fo}}^{x} \mathrm{d}x\,\lambda \right)^{-1}. \tag{3.36}$$

The initial abundance $Y(x_{\rm fo})$ can be usually neglected. The density parameter of the frozen out particles is then

$$\Omega h^2 \approx \frac{1.54 \times 10^{-10}}{\mathrm{GeV}^2} \frac{g_*^{1/2}(x_{\rm fo})}{g_{*s}(x_{\rm fo})} \left(\int_{x_{\rm fo}}^{x} \mathrm{d}x\, x^{-2} \langle \sigma\, v_{\rm Møl} \rangle \right)^{-1}. \tag{3.37}$$

3.2.4 Freeze-in and other means of thermal particle production

Freeze-in may take place if the interaction between visible and dark sectors is so weak that chemical equilibrium between these sectors is never reached [130]. Particles of the visible sector may still decay or annihilate into the dark sector and thus populate it. In the simplest scenario DM comprises a single heavy and inert particle species; as the temperature drops below the mass of the DM particles the annihilation of visible particles into the dark sector stops and their abundance can become the DM we see today, see Fig. 3.2. In order to avoid overproduction of DM, the freeze-in must take place long before chemical equilibrium is reached.

In case of freeze-in only DM pair production is relevant. Therefore, the Boltzmann equation (3.22) can approximated by

$$\frac{\mathrm{d}Y}{\mathrm{d}x} \approx +\lambda Y_{eq}^2, \tag{3.38}$$

and therefore

$$Y(x) = \int_{x_{\rm rh}}^{x} \mathrm{d}x\,\lambda Y_{eq}^2, \tag{3.39}$$

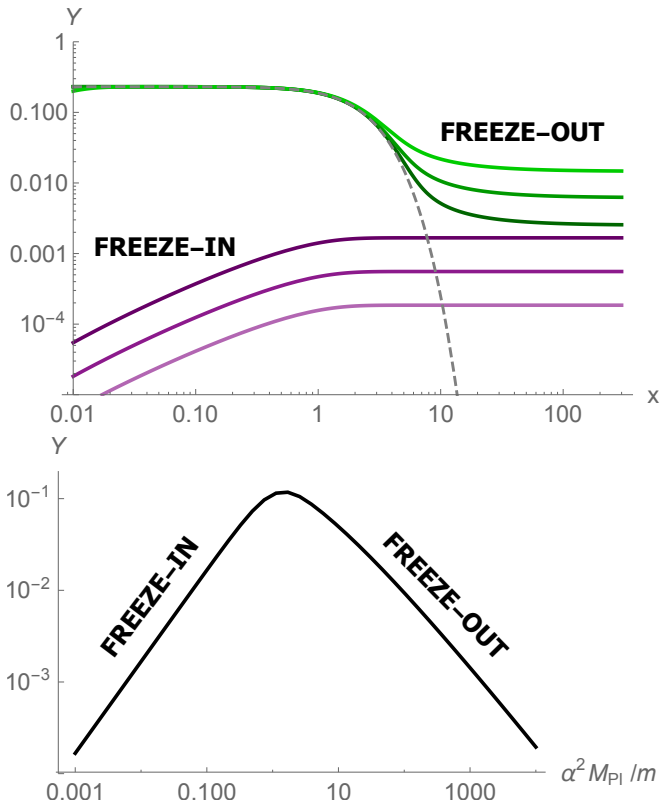

Figure 3.2: An illustrative example of freeze-out and freeze-in of charged fermions from a heat bath of photons. The fermion abundance, expressed by the comoving number density $Y \equiv n/s$, was found by numerically solving the Boltzmann equation (3.22) using the tree level cross section of a QED like theory with a fine structure constant α and fermion mass m. *Upper panel:* The evolution of Y with temperature $x \equiv m/T$. The purple lines correspond to freeze-in and the green lines to freeze-out. In both cases, the lighter the lines the weaker the interactions. The dashed grey line shows the equilibrium abundance. *Lower panel:* the final abundance as a function of the parameters of the theory.

where $x_{\rm rh} \equiv T_{\rm rh}/m$ corresponds to the reheating temperature. Note that, although the parameter λ is proportional to the annihilation cross section, the term λY_{eq}^2 corresponds to pair production because of detailed balance. As Y_{eq} falls off exponentially for $x \gg 1$ the particle production takes place mainly when the particles are relativistic. A good approximation of the present DM abundance is obtained by setting the upper limit of the integral (3.39) to $x_0 = 1.4$. As $\lambda \propto x^{-2}$ most of the abundance will be created at high energies if the cross-section is constant in the UV and a strong dependence on the reheating temperature is expected. However, Eq. (3.33) indicates that in the case of the more usual asymptotic s^{-1} behaviour of the high energy cross section (see e.g. Eqs. (2.14-2.17)), the thermal average scales as x^2 and the relic abundance will be essentially independent of the reheating temperature as long as $x_{\rm rh} \gg 1$. In all, the density parameter resulting from freeze-in reads

$$\Omega h^2 = 7 \times 10^{25} \frac{g^2}{g_{*s} g_*^{1/2}} m^2 \int_{x_{\rm rh}}^{x_0} {\rm d}x \, x^{-2} \langle \sigma \, v_{\rm Møl} \rangle. \tag{3.40}$$

In more involved scenarios the dark sector may contain several particle species whose interactions may influence the final DM abundance [131]. For example, a self-interacting dark sector could produce subsequent periods of freeze-in and freeze-out. A dark sector interacting feebly with the visible sector can be populated through freeze-in after which it takes on a life of its own. It can be in thermal equilibrium with itself, but it will not thermalise with the visible sector. The lightest stable particle of the dark sector is thus the most likely DM candidate and its abundance can be set by its freeze-out that takes place entirely within the dark sector. This mechanism is known as the dark freeze-out [132–139].

As an alteration of the above scenario, the dark freeze-out may take place before the yield from freeze-in is finalised. Because the dark sector has a lower energy density than the visible one, it will also be colder if it is in thermal equilibrium. This makes it possible that DM pair production is kinetically viable in the visible sector but has frozen out in the dark sector. This scenario is dubbed reannihilation because the density of the frozen out particles can become large enough to reinstate their annihilation [132, 133, 140, 141].

3.3 Milli-charged particles and dark matter

The existence of milli-charged particles is already severely constrained. The constraints can be broadly divided into categories based on whether the milli-charged particles are a constituent of DM or not.

Laboratory constraints for milli-charged particles lighter than the electron arise from the invisible decay of orthopositronium [34, 40], Lamb shift [46], vacuum dichroism [42, 43, 142], light-shining-through-the-wall experiments measuring photon to dark photon oscillations [44, 50, 64] or Schwinger pair production of the milli-charge particles [41]. Constraints for heavier milli-charged particles result from various accelerator experiments [30, 32, 39, 41, 49].

Pair production of light milli-charged particles in the hot and dense medium of the interior of stars can carry away energy as they escape. Observational results for the evolution of red-giants, white dwarfs, horizontal-branch stars [32, 33, 35, 36, 51] yield the strongest limit $\epsilon \lesssim 2 \times 10^{-14}$ in the mass range $m \lesssim 10\,\mathrm{keV}$. This bound could be, however, relaxed if there are one or more dark photons [143]. The allowed energy loss of the Supernova 1987A [31, 36] implies $\epsilon \lesssim 2 \times 10^{-9}$ in the mass range $m \lesssim 10\,\mathrm{MeV}$. If photons propagate through astrophysical magnetic fields they can pair-produce light milli-charged particles which can result in the dimming of light from distant supernovae [45] or the distortion of the CMB spectrum [144].

Any process involving a photon or a Z-boson in the s-channel will create milli-charged particles if the centre of mass energy is large enough. Milli-charged particles will thus be produced in the early Universe whenever the temperature exceeds the mass of the particle. Because of the conservation of charge, the lightest particle with a given milli-charge will be stable and thus contribute to the DM abundance. For example, if the milli-charged particles have masses $m_\epsilon < 1\mathrm{MeV}$ and reach thermal equilibrium with the SM, they are excluded purely by their contribution to the effective number of relativistic degrees of freedom. The constraint in the respective mass range is roughly $\epsilon \lesssim 2 \times 10^{-9}$ [36] and, if the milli-charge results from kinetic mixing with a dark photon, a comparable bound applies to an even wider mass range $m_\epsilon \lesssim 1\mathrm{GeV}$ [51, 145].

Depending on the electric charge and mass of the milli-charged particle, it might never reach thermal equilibrium with the SM. If the particle inter-

acts extremely weakly with the SM, their abundance is likely determined by other interactions it might have. For example, in scenarios with a dark $U(1)$ that kinetically mixes with the SM hypercharge, the abundance of milli-charged particles can be set within a dark freeze-out or reannihilation scenario or, even if it thermalises with the SM, the freeze-out can still take place e.g. through its interaction with the dark photon. In all, within a model-independent approach, the abundance of milli-charged particles should in general be treated independently from their charge and mass.

Milli-charged DM will distort the CMB power spectrum if they are tightly coupled to electrons and protons during recombination. Therefore, they may constitute only a small fraction of the DM abundance [38],

$$\Omega_{\rm MCP} h^2 < 0.001, \tag{3.41}$$

whenever the tight coupling condition [37]

$$\epsilon^2 > 5 \times 10^{-11} \frac{\sqrt{\frac{m_\epsilon}{\rm GeV}}}{(1+\frac{m_\epsilon}{m_e})^{-1/2} + (1+\frac{m_\epsilon}{m_p})^{-1/2}} \tag{3.42}$$

is satisfied. Here m_e and m_p denote the mass of an electron or a proton, respectively. For masses $m_\epsilon > 1$MeV this condition is always violated if $\epsilon < 10^{-6}$. A similar constraint on sub-eV from milli-charged particles based on distortion of CMB was found in Ref. [47].

Astrophysical magnetic fields could expel milli-charged DM in the mass range $100\epsilon < m/\text{TeV} < 10^8\epsilon$ from the galactic disc [48, 61]. This effect can significantly soften the bounds from DM direct detection experiments. Magnetic fields can also distort the density profiles of galaxy cluster haloes consisting of milli-charged DM [53].

3.4 Dark electromagnetism and dark plasma

If there is an unbroken $U(1)$ gauge group in the dark sector, it is plausible that it mediates self-interactions of all or a fraction of DM [74, 75]. In this section we assume that the mixing of the photon and the dark photon is negligible, and we focus on the phenomenology of the dark electromagnetic interaction of DM. Notably, the additional pressure from this self-interaction could help to resolve small-scale problems such as the core-cusp problem or the missing-satellites problem.

A massless dark photon inevitably increases $N_{\rm eff}$. $N_{\rm eff}$ may also be affected by dark particles lighter than 20MeV since they freeze out after neutrino decoupling [146]. These contributions to $N_{\rm eff}$ can, however, be significantly suppressed if the dark sector is much cooler than the visible one. The DM self-interactions may also alter the CMB spectrum [147].

We will focus on scenarios where the DM particles carrying the dark charge do not form bound states e.g. as in models of asymmetric DM that may form dark atoms [148–150]. If DM is composed of particle–antiparticle pairs carrying a dark charge it will form a plasma for a wide range of masses and couplings [27].

Counter-streaming plasmas experience plasma instabilities. To estimate the timescale of shock formation consider the properties of a DM halo in which a fraction comprises charged particle–antiparticle pairs forming a plasma. There are various basic scales of the dark plasma. The Debye length,

$$\lambda_D = \sqrt{\frac{T}{4\pi\alpha_D n}}, \tag{3.43}$$

is the distance at which the electrostatic potential of a charge is screened. Here α_D denotes the fine structure constant of dark electromagnetism, n is the density of dark charge carriers and T is their temperature. The number of charges within a sphere of radius of a Debye length,

$$\Lambda = \frac{4\pi}{3}\lambda_D^3 n \tag{3.44}$$

is dubbed the plasma parameter. A large plasma parameter indicates a weakly coupled plasma dominated by collective effects. The characteristic time scale of these effects is given by the inverse of the plasma frequency

$$\omega_p^{-1} = \sqrt{\frac{m_D}{4\pi\alpha_D n}} = \lambda_D\sqrt{\frac{m_D}{T}}. \tag{3.45}$$

The formation time of a shock depends on the type of the dominant instability. The astrophysical dark plasma is a cold pair plasma. In a situation where two of such plasmas with a comparable density counter-stream, the fastest growing instability mode is the two-stream mode for which the instability growth rate is of the order of the plasma frequency [151]. A

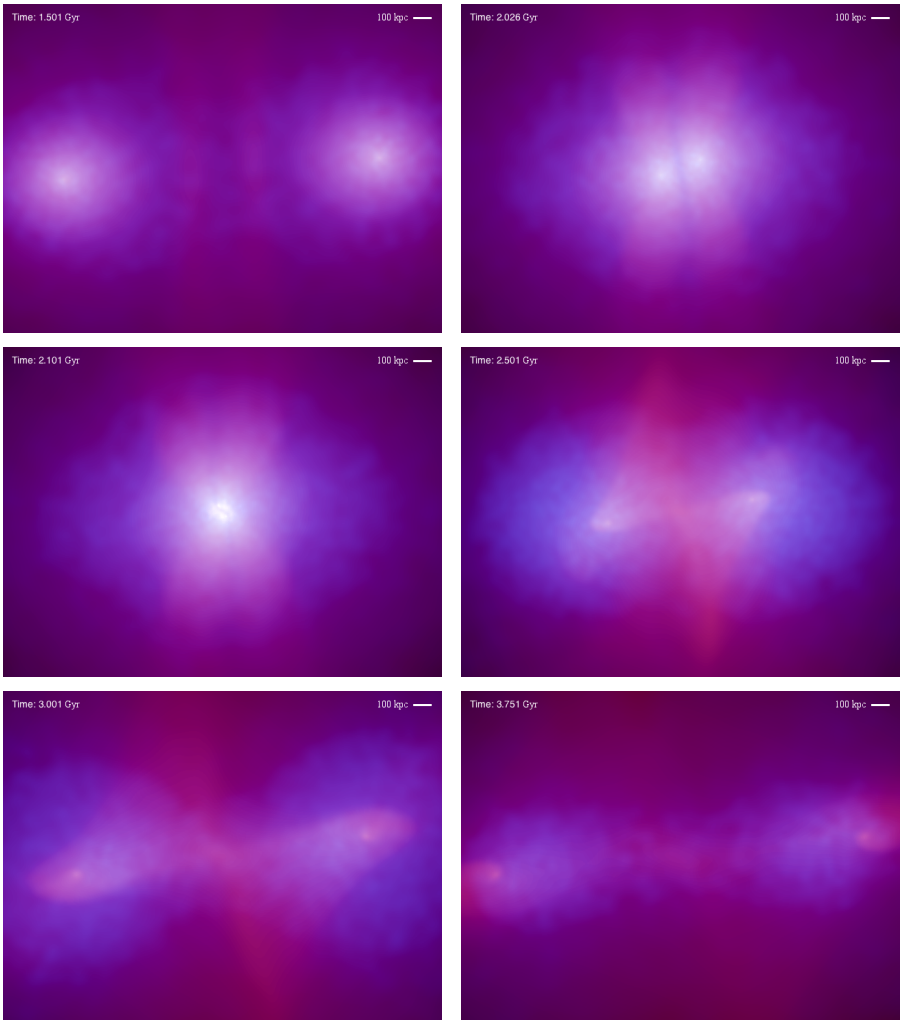

Figure 3.3: Simulation of Abell 520 cluster with 25% of DM acting as a collisional fluid (artificial viscosity $\eta = 0.7$). The non-interacting DM is displayed in blue and the dark plasma in red. The field of view is 2.35 Mpc $\times$ 1.76 Mpc. The corresponding video is available at `http://coe.kbfi.ee/pmwiki/pmwiki.php/Results/Results`. Picture taken from Ref. [28]

conservative estimate of the time it takes to form a shock front is

$$\tau_s \approx 10^3 \omega_p^{-1} = 7\,\mathrm{s} \times \left(\frac{m}{\mathrm{GeV}}\right) \left(\frac{\alpha_D}{10^{-2}}\right)^{-\frac{1}{2}} \left(\frac{\rho_{DP}}{10^{-2}\,\mathrm{GeV/cm^3}}\right)^{-\frac{1}{2}}, \quad (3.46)$$

where ρ_{DP} is the density of the dark plasma component. For a wide range of model parameters, this timescale is much smaller than typical timescales in astrophysics. It is thus expected that the shocks are a prevalent phenomenon in the dynamics of the dark plasma component. Especially, the shocking behaviour is present even if the particles are much heavier and/or the dark fine structure constant much smaller than their counterparts in the visible astrophysical plasmas. The latter allows to suppress radiative cooling that could, for example, lead to the collapse of the dark plasma haloes into dark disks.

The plasma instabilities can thermalise the dark plasma component even if direct collisions between the dark plasma particles are rare [152]. Under the assumption of local thermal equilibrium, this component can be modelled as a collisional fluid. The Bullet Cluster indicates that no more than a third of the mass of the smaller cluster could have been lost. So, all of DM can not exist as a collisional plasma.

In Ref. [28] we tested some of the astrophysical implications of the hypothesis that a subcomponent of DM is collisional by simulating the Abell 520 and the Bullet cluster under idealised conditions. A run of a simulation of the Abell 520 cluster is shown in Fig. 3.3 in a setup where 25% of DM comprises the dark plasma. We used the GADGET-2 code [153] that is based on smoothed-particle hydrodynamics.

4 Summary

Dark matter with long range vector-mediated interactions

Despite the remarkable success of the two standard models of contemporary physics, the ΛCDM and the Standard Model of particle physics, the nature of dark matter remains an open problem. In this thesis we considered scenarios in which all or a part of dark matter may have long range interactions mediated by a vector boson.

The models can be divided into two broad categories. In the first case the mediator is the visible photon and thus the hidden sector contains milli-charged particles. In the second case the mediator is a dark photon giving rise to dark electromagnetism, so it is possible for dark matter to be in a plasma state. The plasma instabilities can make such a dark matter collisional even if the hard collisions of the dark particles are negligible on astrophysical scales. These two categories are not mutually exclusive.

In the first publication [76] we studied milli-charged particles with spin-1. Before, only spin-0 and spin-1/2 milli-charged particles were considered in the literature. We proposed a minimal model of fundamental vector milli-charged particles that is unitary and renormalizable. Unitarity implies that the milli-charged vector is a non-abelian gauge boson with a mass generated by spontaneous symmetry breaking. In the minimal set-up an additional dark $SU(2)_D$ gauge group has to be appended to the $U(1)_Y \times SU(2)_L \times SU(3)_c$ gauge group of the SM together with an hidden scalar charged under $SU(2)_D$. To generate a milli-charge for the dark vector bosons, the dark scalar needs to carry a small hypercharge. The milli-charged vector bosons are stable due to their small electric charge and thus provide a possible DM candidate that may be created by freeze-in. We considered phenomenological implications of this scenario.

The production of milli-charged particles with different spins in photon-photon collisions was considered in the second publication [77]. We showed how the polarisation asymmetries can be a used to measure the spin of the

produced milli-charged particles and discussed a dedicated photon-photon collision experiment.

In the third publication [27] we showed that, if a component of dark matter is charged under a unbroken dark $U(1)$ gauge group, collective plasma effects need to be taken into account to describe its dynamics. For a wide range of model parameters, the plasma effects can thermalise this dark matter component and cause it to behave as a collisional fluid. Similarly to visible astrophysical plasmas, this remains true if the contribution from hard binary collisions between the dark plasma particles are practically negligible.

We proposed a minimal model of dark plasma: it comprises a massless dark photon and a massive dark fermion charged under it. The relic abundance of the dark fermion is produced by thermal freeze-out.

Astrophysical observations rule out the possibility that all dark matter behaves as a collisional fluid. On the other hand, self-interacting dark matter has been proposed as a solution to the small-scale problems of the ΛCDM model, e.g. to the core-cusp problem. It might also explain the central clump observed in the Abell 520 galaxy cluster by gravitational lensing. To test this hypothesis we simulated the Bullet Custer and the Abell 520 cluster in a fourth publication [28] using GADGET-2. We found that the observed features of both the Bullet and Abell 520 cluster can be qualitatively reproduced if a subcomponent of dark matter behaves as a collisional fluid.

5 Kokkuvõte

Elektromagnetisimi tüüpi vastastikmõjuga tumeaine

Hoolimata kaasaegse füüsika kahe olulisima standardmudeli, elementaarosakeste füüsika standardmudeli ja ΛCDM-mudeli, märkimisväärsest edust on tumeaine olemus endiselt lahtine probleem. Käesolevas väitekirjas käsitleti tumeaine mudeleid, milles tumeaine osaleb elektromagnetismi tüüpi lõputu mõjuraadiusega vastastikmõjus.

Seda tüüpi mudelid võib jagada kahte laia kategooriasse. Esiteks võib vastasmõju vahendajaks olla standardmudeli footon, mis tähendab, et tumeda sektori osakesed võivad kanda väikest elektrilaengut ehk millilaengut. Teisel juhul saame rääkida tumedast footonist, mis vahendab tumedat elektromagnetilist interaktsiooni, milles nähtav aine ei osale. Tumedat laengut kandvatest osakestest koosnev tumeaine saab olla plasma olekus. Plasmale omased ebastabiilsused suudavad sellise tumeaine termaliseerida ka olukorras, kus osakestevahelised põrked on väga harvad. Need kaks kategooriat ei välista teineteist.

Esimeses publikatsioonis [76] uurisime millilaetud osakesi spinniga 1. Eelnevalt oli kirjanduses käsitletud vaid millilaetud osakesi spinnidega 0 ja 1/2. Konstrueerisime millilaetud vektorbosonite minimaalse mudeli, mis on unitaarse ja renormeeritav. Unitaarsusest järeldub, et laetud vektorbosonid on mõne mitte-Abeli kalibratsioonirühma kalibratsioonibosonid, mille mass on tekitatud sponataanse sümmeetria rikkumise teel. Lihtsaimas mudelis lisandub standardmudeli kalibratsioonirühmale $U(1)_Y \times SU(2)_L \times SU(3)_c$ tumeda sektori $SU(2)_D$ kalibratsioonirühm koos tumeda skalaarväljaga, mis on viimase all laetud. Millilaengu genereerimiseks peab see skalaar kandma ka väikest hüperlaengut. Elektrilaengu jäävuse tõttu on väikese elektrilaenguga vektorbosonid stabiilsed. Järelikult on taoline osake võimalik tumeaine kandidaat, mis võib varajases universumis tekkida sissekülmumise teel. Uurisime selle mudeli fenomenoloogiat.

Teises publikatsioonis [77] käsitlesime erineva spinniga millilaetud osa-

keste paariteket footonite põrgetes. Näitasime, kuidas kasutada polarisatsiooni asümmeetriat tekkivate millilaetud osakeste spinni mõõtmiseks ja pakkusime välja footonite põrgetel põhineva eksperimendi.

Kolmandas artiklis [27] näitasime, et kui mõni tumeaine komponent on laetud rikkumata $U(1)$ kalibratsioonirühma all, siis tuleb selle komponendi dünaamika kirjeldamisel arvestada kollektiivsete plasma efektidega. Lööklainete tekkimine selliste plasmade põrgetel on võimalik väga laias tumeaine osakeste masside ja laengute vahemikus. Sarnaselt nähtavate astrofüüsikaliste plasmadega suudavad need lööklained tumeaine termaliseerida, isegi kui osakestevahelisi põrkeid praktiliselt ei toimu.

Pakkusime välja tumeda plasma minimaalse mudeli: see sisaldab massitut tumedat footonit ja fermioni, mis viimasega vastastikmõjustub. Tumeaine moodustamiseks vajalik kogus tumedaid fermione tekitatakse väljakülmumise teel.

Astronoomilistest ja kosmoloogilistest vaatlustest järeldub, et tumeaine ei saa iseendaga liiga tugevalt interakteeruda. Teisest küljest võib tumeaine omavastastikmõju lahendada ΛCDM-mudeli väikese skaala probleemid. Samuti võib see seletada galaktikaparvest Abell 520 gravitatsiooniläätse efekti abil leitud keskmist massikontsentratsiooni, mis, juhul kui osa tumeainest iseendaga interakteerub, võis sinna maha jääda galaktikaparvede põrkel. Viimase hüpoteesi testimiseks viisime neljandas publikatsioonis [28] läbi galaktikaparvede Abell 520 ja 1E 0657-558 simulatsiooni, kasutades tarkvara GADGET-2. Leidsime, et mõlema galaktikaparve iseärasused on kvalitatiivselt reprodutseeritavad, kui osa tumeainest iseendaga interakteerub.

Acknowledgements

I would like to thank my thesis supervisor and group leader Martti Raidal for his guidance and continuous collaboration and my co-supervisors Stefan Groote and Emidio Gabrielli for their input and support. I would like to express my gratitude for my colleagues in the particle physics group of the National Institute of Chemical Physics and Biophyiscs for valuable physics discussions and for creating a enjoyable working environment.

This work was supported by the grant IUT23-6 and by EU through the ERDF CoE program grant TK133.

Bibliography

[1] C. Patrignani et al. Review of Particle Physics. *Chin. Phys.*, C40(10):100001, 2016.

[2] P. A. R. Ade et al. Planck 2015 results. XIII. Cosmological parameters. *Astron. Astrophys.*, 594:A13, 2016.

[3] Gianfranco Bertone, Dan Hooper, and Joseph Silk. Particle dark matter: Evidence, candidates and constraints. *Phys. Rept.*, 405:279–390, 2005.

[4] Jonathan L. Feng. Dark Matter Candidates from Particle Physics and Methods of Detection. *Ann. Rev. Astron. Astrophys.*, 48:495–545, 2010.

[5] M. Markevitch, A. H. Gonzalez, L. David, A. Vikhlinin, S. Murray, W. Forman, C. Jones, and W. Tucker. A Textbook example of a bow shock in the merging galaxy cluster 1E0657-56. *Astrophys. J.*, 567:L27, 2002.

[6] Maxim Markevitch, A. H. Gonzalez, D. Clowe, A. Vikhlinin, L. David, W. Forman, C. Jones, S. Murray, and W. Tucker. Direct constraints on the dark matter self-interaction cross-section from the merging galaxy cluster 1E0657-56. *Astrophys. J.*, 606:819–824, 2004.

[7] Volker Springel and Glennys Farrar. The Speed of the bullet in the merging galaxy cluster 1E0657-56. *Mon. Not. Roy. Astron. Soc.*, 380:911–925, 2007.

[8] Bernard Carr, Florian Kuhnel, and Marit Sandstad. Primordial Black Holes as Dark Matter. *Phys. Rev.*, D94(8):083504, 2016.

[9] Bernard Carr, Martti Raidal, Tommi Tenkanen, Ville Vaskonen, and Hardi Veermäe. Primordial black hole constraints for extended mass functions. *Phys. Rev.*, D96(2):023514, 2017.

[10] Gerard Jungman, Marc Kamionkowski, and Kim Griest. Supersymmetric dark matter. *Phys. Rept.*, 267:195–373, 1996.

[11] Leszek Roszkowski, Enrico Maria Sessolo, and Sebastian Trojanowski. WIMP dark matter candidates and searches - current issues and future prospects. 2017.

[12] Scott W. Randall, Maxim Markevitch, Douglas Clowe, Anthony H. Gonzalez, and Marusa Bradac. Constraints on the Self-Interaction Cross-Section of Dark Matter from Numerical Simulations of the Merging Galaxy Cluster 1E 0657-56. *Astrophys. J.*, 679:1173–1180, 2008.

[13] Annika H. G. Peter, Miguel Rocha, James S. Bullock, and Manoj Kaplinghat. Cosmological Simulations with Self-Interacting Dark Matter II: Halo Shapes vs. Observations. *Mon. Not. Roy. Astron. Soc.*, 430:105, 2013.

[14] Miguel Rocha, Annika H. G. Peter, James S. Bullock, Manoj Kaplinghat, Shea Garrison-Kimmel, Jose Onorbe, and Leonidas A. Moustakas. Cosmological Simulations with Self-Interacting Dark Matter I: Constant Density Cores and Substructure. *Mon. Not. Roy. Astron. Soc.*, 430:81–104, 2013.

[15] B. Moore, S. Ghigna, F. Governato, G. Lake, Thomas R. Quinn, J. Stadel, and P. Tozzi. Dark matter substructure within galactic halos. *Astrophys. J.*, 524:L19–L22, 1999.

[16] Anatoly A. Klypin, Andrey V. Kravtsov, Octavio Valenzuela, and Francisco Prada. Where are the missing Galactic satellites? *Astrophys. J.*, 522:82–92, 1999.

[17] Ben Moore, Thomas R. Quinn, Fabio Governato, Joachim Stadel, and George Lake. Cold collapse and the core catastrophe. *Mon. Not. Roy. Astron. Soc.*, 310:1147–1152, 1999.

[18] W. J. G. de Blok. The Core-Cusp Problem. *Advances in Astronomy*, 2010:789293, 2010.

[19] Michael Boylan-Kolchin, James S. Bullock, and Manoj Kaplinghat. Too big to fail? The puzzling darkness of massive Milky Way subhaloes. *Mon. Not. Roy. Astron. Soc.*, 415:L40, 2011.

[20] Michael Boylan-Kolchin, James S. Bullock, and Manoj Kaplinghat. The Milky Way's bright satellites as an apparent failure of LCDM. *Mon. Not. Roy. Astron. Soc.*, 422:1203–1218, 2012.

[21] Sean Tulin, Hai-Bo Yu, and Kathryn M. Zurek. Beyond Collisionless Dark Matter: Particle Physics Dynamics for Dark Matter Halo Structure. *Phys. Rev.*, D87(11):115007, 2013.

[22] Sean Tulin and Hai-Bo Yu. Dark Matter Self-interactions and Small Scale Structure. 2017.

[23] A. Mahdavi, H. y Hoekstra, A. y Babul, D. y Balam, and P. Capak. A Dark Core in Abell 520. *Astrophys. J.*, 668:806–814, 2007.

[24] M. James Jee, Henk Hoekstra, Andisheh Mahdavi, and Arif Babul. Hubble Space Telescope/Advanced Camera for Surveys Confirmation of the Dark Substructure in A520. *Astrophys. J.*, 783:78, 2014.

[25] M. J. Jee, A. Mahdavi, H. Hoekstra, A. Babul, J. J. Dalcanton, P. Carroll, and P. Capak. A Study of the Dark Core in A520 with Hubble Space Telescope: The Mystery Deepens. *Astrophys. J.*, 747:96, 2012.

[26] Nobuhiro Okabe and Keiichi Umetsu. Subaru Weak Lensing Study of Seven Merging Clusters: Distributions of Mass and Baryons. *Publ. Astron. Soc. Jap.*, 60:345, 2008.

[27] Matti Heikinheimo, Martti Raidal, Christian Spethmann, and Hardi Veermäe. Dark matter self-interactions via collisionless shocks in cluster mergers. *Phys. Lett.*, B749:236–241, 2015.

[28] Tiit Sepp, Boris Deshev, Matti Heikinheimo, Andi Hektor, Martti Raidal, Christian Spethmann, Elmo Tempel, and Hardi Veermäe. Simulations of Galaxy Cluster Collisions with a Dark Plasma Component. 2016.

[29] Haim Goldberg and Lawrence J. Hall. A New Candidate for Dark Matter. *Phys. Lett.*, B174:151, 1986. [,467(1986)].

[30] E. Golowich and R. W. Robinett. Limits on Millicharged Matter From Beam Dump Experiments. *Phys. Rev.*, D35:391, 1987.

[31] R. N. Mohapatra and I. Z. Rothstein. Astrophysical constraints on minicharged particles. *Phys. Lett.*, B247:593–600, 1990.

[32] S. Davidson, B. Campbell, and David C. Bailey. Limits on particles of small electric charge. *Phys. Rev.*, D43:2314–2321, 1991.

[33] Sacha Davidson and Michael E. Peskin. Astrophysical bounds on millicharged particles in models with a paraphoton. *Phys. Rev.*, D49:2114–2117, 1994.

[34] T. Mitsui, R. Fujimoto, Y. Ishisaki, Y. Ueda, Y. Yamazaki, S. Asai, and S. Orito. Search for invisible decay of orthopositronium. *Phys. Rev. Lett.*, 70:2265–2268, 1993.

[35] G. G. Raffelt. *Stars as laboratories for fundamental physics*. 1996.

[36] Sacha Davidson, Steen Hannestad, and Georg Raffelt. Updated bounds on millicharged particles. *JHEP*, 05:003, 2000.

[37] S. L. Dubovsky, D. S. Gorbunov, and G. I. Rubtsov. Narrowing the window for millicharged particles by CMB anisotropy. *JETP Lett.*, 79:1–5, 2004. [Pisma Zh. Eksp. Teor. Fiz.79,3(2004)].

[38] A. D. Dolgov, S. L. Dubovsky, G. I. Rubtsov, and I. I. Tkachev. Constraints on millicharged particles from Planck data. *Phys. Rev.*, D88(11):117701, 2013.

[39] A. A. Prinz et al. Search for millicharged particles at SLAC. *Phys. Rev. Lett.*, 81:1175–1178, 1998.

[40] A. Badertscher, P. Crivelli, W. Fetscher, U. Gendotti, S. Gninenko, V. Postoev, A. Rubbia, V. Samoylenko, and D. Sillou. An Improved Limit on Invisible Decays of Positronium. *Phys. Rev.*, D75:032004, 2007.

[41] H. Gies, J. Jaeckel, and A. Ringwald. Accelerator Cavities as a Probe of Millicharged Particles. *Europhys. Lett.*, 76:794–800, 2006.

[42] S. N. Gninenko, N. V. Krasnikov, and A. Rubbia. Search for millicharged particles in reactor neutrino experiments: A Probe of the PVLAS anomaly. *Phys. Rev.*, D75:075014, 2007.

[43] Markus Ahlers, Holger Gies, Joerg Jaeckel, and Andreas Ringwald. On the Particle Interpretation of the PVLAS Data: Neutral versus Charged Particles. *Phys. Rev.*, D75:035011, 2007.

[44] M. Ahlers, H. Gies, J. Jaeckel, J. Redondo, and A. Ringwald. Light from the hidden sector. *Phys. Rev.*, D76:115005, 2007.

[45] Markus Ahlers. The Hubble diagram as a probe of mini-charged particles. *Phys. Rev.*, D80:023513, 2009.

[46] M. Gluck, S. Rakshit, and E. Reya. The Lamb shift contribution of very light milli-charged fermions. *Phys. Rev.*, D76:091701, 2007.

[47] Alessandro Melchiorri, Antonello Polosa, and Alessandro Strumia. New bounds on millicharged particles from cosmology. *Phys. Lett.*, B650:416–420, 2007.

[48] Samuel D. McDermott, Hai-Bo Yu, and Kathryn M. Zurek. Turning off the Lights: How Dark is Dark Matter? *Phys. Rev.*, D83:063509, 2011.

[49] Joerg Jaeckel, Martin Jankowiak, and Michael Spannowsky. LHC probes the hidden sector. *Phys. Dark Univ.*, 2:111–117, 2013.

[50] Babette Döbrich, Holger Gies, Norman Neitz, and Felix Karbstein. Magnetically amplified light-shining-through-walls via virtual minicharged particles. *Phys. Rev.*, D87(2):025022, 2013.

[51] Hendrik Vogel and Javier Redondo. Dark Radiation constraints on minicharged particles in models with a hidden photon. *JCAP*, 1402:029, 2014.

[52] Prateek Agrawal, Francis-Yan Cyr-Racine, Lisa Randall, and Jakub Scholtz. Make Dark Matter Charged Again. *JCAP*, 1705(05):022, 2017.

[53] Kenji Kadota, Toyokazu Sekiguchi, and Hiroyuki Tashiro. A new constraint on millicharged dark matter from galaxy clusters. 2016.

[54] H. Georgi and S. L. Glashow. Unity of All Elementary Particle Forces. *Phys. Rev. Lett.*, 32:438–441, 1974.

[55] Paul A. M. Dirac. Quantized Singularities in the Electromagnetic Field. *Proc. Roy. Soc. Lond.*, A133:60–72, 1931.

[56] Bob Holdom. Two U(1)'s and Epsilon Charge Shifts. *Phys. Lett.*, B166:196–198, 1986.

[57] A. De Rujula, S. L. Glashow, and U. Sarid. CHARGED DARK MATTER. *Nucl. Phys.*, B333:173–194, 1990.

[58] James M. Cline, Zuowei Liu, and Wei Xue. Millicharged Atomic Dark Matter. *Phys. Rev.*, D85:101302, 2012.

[59] Chris Kouvaris. Composite Millicharged Dark Matter. *Phys. Rev.*, D88(1):015001, 2013.

[60] Audrey K. Kvam and David C. Latimer. Astrophysical constraints on millicharged atomic dark matter. 2014.

[61] Leonid Chuzhoy and Edward W. Kolb. Reopening the window on charged dark matter. *JCAP*, 0907:014, 2009.

[62] M. Ahlers, H. Gies, J. Jaeckel, J. Redondo, and A. Ringwald. Laser experiments explore the hidden sector. *Phys. Rev.*, D77:095001, 2008.

[63] L. B. Okun. Limits of electrodynamics: paraphotons? *Sov. Phys. JETP*, 56:502, 1982. [Zh. Eksp. Teor. Fiz.83,892(1982)].

[64] Steven A. Abel, Joerg Jaeckel, Valentin V. Khoze, and Andreas Ringwald. Illuminating the Hidden Sector of String Theory by Shining Light through a Magnetic Field. *Phys. Lett.*, B666:66–70, 2008.

[65] S. A. Abel, M. D. Goodsell, J. Jaeckel, V. V. Khoze, and A. Ringwald. Kinetic Mixing of the Photon with Hidden U(1)s in String Phenomenology. *JHEP*, 07:124, 2008.

[66] Keith R. Dienes, Christopher F. Kolda, and John March-Russell. Kinetic mixing and the supersymmetric gauge hierarchy. *Nucl. Phys.*, B492:104–118, 1997.

[67] Andre Lukas and K. S. Stelle. Heterotic anomaly cancellation in five-dimensions. *JHEP*, 01:010, 2000.

[68] D. Lust and S. Stieberger. Gauge threshold corrections in intersecting brane world models. *Fortsch. Phys.*, 55:427–465, 2007.

[69] S. A. Abel and B. W. Schofield. Brane anti-brane kinetic mixing, millicharged particles and SUSY breaking. *Nucl. Phys.*, B685:150–170, 2004.

[70] Ralph Blumenhagen, Gabriele Honecker, and Timo Weigand. Loop-corrected compactifications of the heterotic string with line bundles. *JHEP*, 06:020, 2005.

[71] Ralph Blumenhagen, Sebastian Moster, and Timo Weigand. Heterotic GUT and standard model vacua from simply connected Calabi-Yau manifolds. *Nucl. Phys.*, B751:186–221, 2006.

[72] Javier Redondo and Marieke Postma. Massive hidden photons as lukewarm dark matter. *JCAP*, 0902:005, 2009.

[73] Maxim Pospelov, Adam Ritz, and Mikhail B. Voloshin. Bosonic super-WIMPs as keV-scale dark matter. *Phys. Rev.*, D78:115012, 2008.

[74] Lotty Ackerman, Matthew R. Buckley, Sean M. Carroll, and Marc Kamionkowski. Dark Matter and Dark Radiation. *Phys. Rev.*, D79:023519, 2009. [,277(2008)].

[75] Jonathan L. Feng, Manoj Kaplinghat, Huitzu Tu, and Hai-Bo Yu. Hidden Charged Dark Matter. *JCAP*, 0907:004, 2009.

[76] Emidio Gabrielli, Luca Marzola, Martti Raidal, and Hardi Veermäe. Dark matter and spin-1 milli-charged particles. *JHEP*, 08:150, 2015.

[77] Emidio Gabrielli, Luca Marzola, Edoardo Milotti, and Hardi Veermäe. Polarization observables for millicharged particles in photon collisions. *Phys. Rev.*, D94(9):095014, 2016.

[78] L. D. Faddeev and V. N. Popov. Feynman Diagrams for the Yang-Mills Field. *Phys. Lett.*, 25B:29–30, 1967.

[79] Peter W. Higgs. Broken symmetries and the masses of gauge bosons. *Phys. Rev. Lett.*, 13:508–509, Oct 1964.

[80] G. S. Guralnik, C. R. Hagen, and T. W. B. Kibble. Global conservation laws and massless particles. *Phys. Rev. Lett.*, 13:585–587, Nov 1964.

[81] F. Englert and R. Brout. Broken symmetry and the mass of gauge vector mesons. *Phys. Rev. Lett.*, 13:321–323, Aug 1964.

[82] Sergio Ferrara, Massimo Porrati, and Valentine L. Telegdi. g = 2 as the natural value of the tree level gyromagnetic ratio of elementary particles. *Phys. Rev.*, D46:3529–3537, 1992.

[83] C. H. Llewellyn Smith. High-Energy Behavior and Gauge Symmetry. *Phys. Lett.*, B46:233–236, 1973.

[84] John M. Cornwall, David N. Levin, and George Tiktopoulos. Derivation of Gauge Invariance from High-Energy Unitarity Bounds on the s Matrix. *Phys. Rev.*, D10:1145, 1974. [Erratum: Phys. Rev.D11,972(1975)].

[85] John M. Cornwall and George Tiktopoulos. On-Shell Asymptotics of Nonabelian Gauge Theories. *Phys. Rev. Lett.*, 35:338, 1975.

[86] Jeffrey Goldstone, Abdus Salam, and Steven Weinberg. Broken symmetries. *Phys. Rev.*, 127:965–970, Aug 1962.

[87] William A. Bardeen, R. Gastmans, and B. E. Lautrup. Static quantities in Weinberg's model of weak and electromagnetic interactions. *Nucl. Phys.*, B46:319–331, 1972.

[88] K. J. F. Gaemers and G. J. Gounaris. Polarization Amplitudes for e+ e- -¿ W+ W- and e+ e- -¿ Z Z. *Z. Phys.*, C1:259, 1979.

[89] Kaoru Hagiwara, R. D. Peccei, D. Zeppenfeld, and K. Hikasa. Probing the Weak Boson Sector in e+ e- —¿ W+ W-. *Nucl. Phys.*, B282:253–307, 1987.

[90] Gerard 't Hooft and M. J. G. Veltman. Regularization and Renormalization of Gauge Fields. *Nucl. Phys.*, B44:189–213, 1972.

[91] Howard Georgi and Sheldon L. Glashow. Unified weak and electromagnetic interactions without neutral currents. *Phys. Rev. Lett.*, 28:1494, 1972.

[92] Boris Kors and Pran Nath. A Stueckelberg extension of the standard model. *Phys. Lett.*, B586:366–372, 2004.

[93] Boris Kors and Pran Nath. Aspects of the Stueckelberg extension. *JHEP*, 07:069, 2005.

[94] Daniel Feldman, Zuowei Liu, and Pran Nath. The Stueckelberg Z-prime Extension with Kinetic Mixing and Milli-Charged Dark Matter From the Hidden Sector. *Phys. Rev.*, D75:115001, 2007.

[95] Kingman Cheung and Tzu-Chiang Yuan. Hidden fermion as milli-charged dark matter in Stueckelberg Z- prime model. *JHEP*, 03:120, 2007.

[96] F. Zwicky. Die Rotverschiebung von extragalaktischen Nebeln. *Helv. Phys. Acta*, 6:110–127, 1933. [Gen. Rel. Grav.41,207(2009)].

[97] H. W. Babcock. The rotation of the Andromeda Nebula. *Lick Observatory Bulletin*, 19:41–51, 1939.

[98] V. C. Rubin and W. K. Ford, Jr. Rotation of the Andromeda Nebula from a Spectroscopic Survey of Emission Regions. *Astrophysical Journal*, 159:379, February 1970.

[99] M. S. Roberts and R. N. Whitehurst. The rotation curve and geometry of M31 at large galactocentric distances. *Astrophysical Journal*, 201:327–346, October 1975.

[100] Albert Einstein. Lens-Like Action of a Star by the Deviation of Light in the Gravitational Field. *Science*, 84:506–507, 1936.

[101] F. Zwicky. Nebulae as gravitational lenses. *Phys. Rev.*, 51:290, 1937.

[102] Simon D. M. White, Julio F. Navarro, August E. Evrard, and Carlos S. Frenk. The Baryon content of galaxy clusters: A Challenge to cosmological orthodoxy. *Nature*, 366:429–433, 1993.

[103] W. H. Tucker, H. Tananbaum, and R. A. Remillard. A search for 'failed clusters' of galaxies. *Astrophysical Journal*, 444:532–547, May 1995.

[104] Maxim Markevitch. Chandra observation of the most interesting cluster in the universe. 2005. [ESA Spec. Publ.604,723(2006)].

[105] Douglas Clowe, Marusa Bradac, Anthony H. Gonzalez, Maxim Markevitch, Scott W. Randall, Christine Jones, and Dennis Zaritsky. A direct empirical proof of the existence of dark matter. *Astrophys. J.*, 648:L109–L113, 2006.

[106] P. A. R. Ade et al. Planck 2013 results. XVI. Cosmological parameters. *Astron. Astrophys.*, 571:A16, 2014.

[107] Adam G. Riess, Lucas Macri, Stefano Casertano, Hubert Lampeitl, Henry C. Ferguson, Alexei V. Filippenko, Saurabh W. Jha, Weidong Li, and Ryan Chornock. A 3% Solution: Determination of the Hubble Constant with the Hubble Space Telescope and Wide Field Camera 3. *Astrophys. J.*, 730:119, 2011. [Erratum: Astrophys. J.732,129(2011)].

[108] Adam G. Riess et al. A 2.4% Determination of the Local Value of the Hubble Constant. *Astrophys. J.*, 826(1):56, 2016.

[109] H. Hildebrandt et al. KiDS-450: Cosmological parameter constraints from tomographic weak gravitational lensing. *Mon. Not. Roy. Astron. Soc.*, 465:1454, 2017.

[110] Shahab Joudaki et al. KiDS-450: Testing extensions to the standard cosmological model. *Mon. Not. Roy. Astron. Soc.*, 2016.

[111] Jose Luis Bernal, Licia Verde, and Adam G. Riess. The trouble with H_0. *JCAP*, 1610(10):019, 2016.

[112] David H. Weinberg, James S. Bullock, Fabio Governato, Rachel Kuzio de Naray, and Annika H. G. Peter. Cold dark matter: controversies on small scales. *Proc. Nat. Acad. Sci.*, 112:12249–12255, 2014.

[113] Julio F. Navarro, Carlos S. Frenk, and Simon D. M. White. The Structure of cold dark matter halos. *Astrophys. J.*, 462:563–575, 1996.

[114] Kyle A. Oman et al. The unexpected diversity of dwarf galaxy rotation curves. *Mon. Not. Roy. Astron. Soc.*, 452(4):3650–3665, 2015.

[115] Wayne Hu, Rennan Barkana, and Andrei Gruzinov. Cold and fuzzy dark matter. *Phys. Rev. Lett.*, 85:1158–1161, 2000.

[116] Felix Kahlhoefer, Kai Schmidt-Hoberg, Janis Kummer, and Subir Sarkar. On the interpretation of dark matter self-interactions in Abell 3827. *Mon. Not. Roy. Astron. Soc.*, 452(1):L54–L58, 2015.

[117] Felix Kahlhoefer, Kai Schmidt-Hoberg, Mads T. Frandsen, and Subir Sarkar. Colliding clusters and dark matter self-interactions. *Mon. Not. Roy. Astron. Soc.*, 437(3):2865–2881, 2014.

[118] Edward W. Kolb and Michael S. Turner. The Early Universe. *Front. Phys.*, 69:1–547, 1990.

[119] D. J. Fixsen. The Temperature of the Cosmic Microwave Background. *Astrophys. J.*, 707:916–920, 2009.

[120] Jong-Mann Yang, David N. Schramm, Gary Steigman, and Robert T. Rood. Constraints on Cosmology and Neutrino Physics from Big Bang Nucleosynthesis. *Astrophys. J.*, 227:697–704, 1979.

[121] G. Mangano, G. Miele, S. Pastor, and M. Peloso. A Precision calculation of the effective number of cosmological neutrinos. *Phys. Lett.*, B534:8–16, 2002.

[122] Rui-Yun Guo and Xin Zhang. Constraints on inflation revisited: An analysis including the latest local measurement of the Hubble constant. 2017.

[123] Richard H. Cyburt, Brian D. Fields, Keith A. Olive, and Evan Skillman. New BBN limits on physics beyond the standard model from ^4He. *Astropart. Phys.*, 23:313–323, 2005.

[124] Paolo Gondolo and Graciela Gelmini. Cosmic abundances of stable particles: Improved analysis. *Nucl. Phys.*, B360:145–179, 1991.

[125] Kim Griest and Marc Kamionkowski. Unitarity Limits on the Mass and Radius of Dark Matter Particles. *Phys. Rev. Lett.*, 64:615, 1990.

[126] A. Sommerfeld. Über die Beugung und Bremsung der Elektronen. *Annalen der Physik*, 403:257–330, 1931.

[127] Jonathan L. Feng, Manoj Kaplinghat, and Hai-Bo Yu. Sommerfeld Enhancements for Thermal Relic Dark Matter. *Phys. Rev.*, D82:083525, 2010.

[128] Marcel Froissart. Asymptotic behavior and subtractions in the Mandelstam representation. *Phys. Rev.*, 123:1053–1057, 1961.

[129] Michael E. Peskin and Daniel V. Schroeder. *An Introduction to quantum field theory*. Addison-Wesley, Reading, USA, 1995.

[130] Lawrence J. Hall, Karsten Jedamzik, John March-Russell, and Stephen M. West. Freeze-In Production of FIMP Dark Matter. *JHEP*, 03:080, 2010.

[131] Nicolás Bernal, Matti Heikinheimo, Tommi Tenkanen, Kimmo Tuominen, and Ville Vaskonen. The Dawn of FIMP Dark Matter: A Review of Models and Constraints. 2017.

[132] Xiaoyong Chu, Thomas Hambye, and Michel H. G. Tytgat. The Four Basic Ways of Creating Dark Matter Through a Portal. *JCAP*, 1205:034, 2012.

[133] Nicolas Bernal, Xiaoyong Chu, Camilo Garcia-Cely, Thomas Hambye, and Bryan Zaldivar. Production Regimes for Self-Interacting Dark Matter. *JCAP*, 1603(03):018, 2016.

[134] Eric D. Carlson, Marie E. Machacek, and Lawrence J. Hall. Self-interacting dark matter. *Astrophys. J.*, 398:43–52, 1992.

[135] Matti Heikinheimo, Tommi Tenkanen, Kimmo Tuominen, and Ville Vaskonen. Observational Constraints on Decoupled Hidden Sectors. *Phys. Rev.*, D94(6):063506, 2016.

[136] Nicolas Bernal and Xiaoyong Chu. $\mathbb{Z}_2$ SIMP Dark Matter. *JCAP*, 1601:006, 2016.

[137] Nicolás Bernal, Xiaoyong Chu, and Josef Pradler. Simply split strongly interacting massive particles. *Phys. Rev.*, D95(11):115023, 2017.

[138] A. D. Dolgov. On concentration of relict theta particles. (in russian). *Yad. Fiz.*, 31:1522–1528, 1980.

[139] A. D. Dolgov. New Old Mechanism of Dark Matter Burning. 2017.

[140] Clifford Cheung, Gilly Elor, Lawrence J. Hall, and Piyush Kumar. Origins of Hidden Sector Dark Matter I: Cosmology. *JHEP*, 03:042, 2011.

[141] Clifford Cheung, Gilly Elor, Lawrence J. Hall, and Piyush Kumar. Origins of Hidden Sector Dark Matter II: Collider Physics. *JHEP*, 03:085, 2011.

[142] Holger Gies, Joerg Jaeckel, and Andreas Ringwald. Polarized Light Propagating in a Magnetic Field as a Probe of Millicharged Fermions. *Phys. Rev. Lett.*, 97:140402, 2006.

[143] Eduard Masso and Javier Redondo. Compatibility of CAST search with axion-like interpretation of PVLAS results. *Phys. Rev. Lett.*, 97:151802, 2006.

[144] C. Burrage, J. Jaeckel, J. Redondo, and A. Ringwald. Late time CMB anisotropies constrain mini-charged particles. *JCAP*, 0911:002, 2009.

[145] Christopher Brust, David E. Kaplan, and Matthew T. Walters. New Light Species and the CMB. *JHEP*, 12:058, 2013.

[146] Jae Ho Heo and C. S. Kim. Light Dark Matter and Dark Radiation. *J. Korean Phys. Soc.*, 68(5):715–721, 2016.

[147] Francis-Yan Cyr-Racine, Roland de Putter, Alvise Raccanelli, and Kris Sigurdson. Constraints on Large-Scale Dark Acoustic Oscillations from Cosmology. *Phys. Rev.*, D89(6):063517, 2014.

[148] David E. Kaplan, Markus A. Luty, and Kathryn M. Zurek. Asymmetric Dark Matter. *Phys. Rev.*, D79:115016, 2009.

[149] D. E. Kaplan, G. Z. Krnjaic, K. R. Rehermann, and C. M. Wells. Atomic dark matter. *JCAP*, 5:021, May 2010.

[150] Francis-Yan Cyr-Racine and Kris Sigurdson. Cosmology of atomic dark matter. *Phys. Rev.*, D87(10):103515, 2013.

[151] A. Bret. Weibel, Two-Stream, Filamentation, Oblique, Bell, Buneman... which one grows faster ? *Astrophys. J.*, 699:990–1003, 2009.

[152] Antoine Bret. Collisional behaviors of astrophysical collisionless plasmas. *J. Plasma Phys.*, 81(02):455810202, 2015.

[153] Volker Springel. The Cosmological simulation code GADGET-2. *Mon. Not. Roy. Astron. Soc.*, 364:1105–1134, 2005.

Publications

Curriculum Vitae

Hardi Veermäe

Name:	Hardi Veermäe
Date and place of birth:	June 17, 1985, Viljandi, Estonia
Citizenship:	Estonian
Address:	National Institute of Chemical Physics and Biophysics, Akadeemia tee 23, 12618 Tallinn, Estonia
E-mail:	hardi.veermae@cern.ch

Education

2009-2017	PhD in physics (theoretical physics), University of Tartu
2007-2009	MSc in physics (theoretical physics), *cum laude*, University of Tartu
2004-2007	BSc in physics, University of Tartu
1992-2004	Viljandi Paalalinna High School, Estonia

Employment

2010-2016	Teaching assistant, University of Tartu Courses: - Analytical Mechanics (lecturer) - Introduction to Quantum Field Theory (lecturer) - Advanced Quantum Mechanics (teaching assistant)
2010-...	Researcher, National Institute of Chemical Physics and Biophysics

Curriculum Vitae

Hardi Veermäe

Nimi :	Hardi Veermäe
Sünniaeg ja koht:	7. juuni, 1985, Viljandi, Eesti
Kodakondsus:	Eesti
Aadress:	Keemilise ja Bioloogilise Füüsika Instituut, Akadeemia tee 23, 12618 Tallinn, Eesti
E-mail:	hardi.veermae@cern.ch

Haridus

2009-2017	PhD füüsikas (teoreetiline füüsika), Tartu Ülikool
2007-2009	MSc füüsikas (teoreetiline füüsika), *cum laude*, Tartu Ülikool
2004-2007	BSc füüsikas, Tartu Ülikool
1992-2004	Viljandi Paalalinna Gümnaasium, Eesti

Teenistuskäik

2010-2016	Õppeassistant, Tartu Ülikool Kursused: - Analüütiline mehaanika (õppejõud) - Sissejuhatus kvantväljateooriasse (õppejõud) - Kvantmehaanika jätkukutsus (õppeassistant)
2010-...	Teadur, Keemilise ja Bioloogilise Füüsika Instituut

DISSERTATIONES PHYSICAE UNIVERSITATIS TARTUENSIS

1. **Andrus Ausmees.** XUV-induced electron emission and electron-phonon interaction in alkali halides. Tartu, 1991.
2. **Heiki Sõnajalg.** Shaping and recalling of light pulses by optical elements based on spectral hole burning. Tartu, 1991.
3. **Sergei Savihhin.** Ultrafast dynamics of F-centers and bound excitons from picosecond spectroscopy data. Tartu, 1991.
4. **Ergo Nõmmiste.** Leelishalogeniidide röntgenelektronemissioon kiiritamisel footonitega energiaga 70–140 eV. Tartu, 1991.
5. **Margus Rätsep.** Spectral gratings and their relaxation in some low-temperature impurity-doped glasses and crystals. Tartu, 1991.
6. **Tõnu Pullerits.** Primary energy transfer in photosynthesis. Model calculations. Tartu, 1991.
7. **Olev Saks.** Attoampri diapasoonis voolude mõõtmise füüsikalised alused. Tartu, 1991.
8. **Andres Virro.** AlGaAsSb/GaSb heterostructure injection lasers. Tartu, 1991.
9. **Hans Korge.** Investigation of negative point discharge in pure nitrogen at atmospheric pressure. Tartu, 1992.
10. **Jüri Maksimov.** Nonlinear generation of laser VUV radiation for high-resolution spectroscopy. Tartu, 1992.
11. **Mark Aizengendler.** Photostimulated transformation of aggregate defects and spectral hole burning in a neutron-irradiated sapphire. Tartu, 1992.
12. **Hele Siimon.** Atomic layer molecular beam epitaxy of A^2B^6 compounds described on the basis of kinetic equations model. Tartu, 1992.
13. **Tõnu Reinot.** The kinetics of polariton luminescence, energy transfer and relaxation in anthracene. Tartu, 1992.
14. **Toomas Rõõm.** Paramagnetic H^{2-} and F^+ centers in CaO crystals: spectra, relaxation and recombination luminescence. Tallinn, 1993.
15. **Erko Jalviste.** Laser spectroscopy of some jet-cooled organic molecules. Tartu, 1993.
16. **Alvo Aabloo.** Studies of crystalline celluloses using potential energy calculations. Tartu, 1994.
17. **Peeter Paris.** Initiation of corona pulses. Tartu, 1994.
18. **Павел Рубин.** Локальные дефектные состояния в CuO_2 плоскостях высокотемпературных сверхпроводников. Тарту, 1994.
19. **Olavi Ollikainen.** Applications of persistent spectral hole burning in ultrafast optical neural networks, time-resolved spectroscopy and holographic interferometry. Tartu, 1996.
20. **Ülo Mets.** Methodological aspects of fluorescence correlation spectroscopy. Tartu, 1996.
21. **Mikhail Danilkin.** Interaction of intrinsic and impurity defects in CaS:Eu luminophors. Tartu, 1997.

22. **Ирина Кудрявцева.** Создание и стабилизация дефектов в кристаллах KBr, KCl, RbCl при облучении ВУФ-радиацией. Тарту, 1997.
23. **Andres Osvet.** Photochromic properties of radiation-induced defects in diamond. Tartu, 1998.
24. **Jüri Örd.** Classical and quantum aspects of geodesic multiplication. Tartu, 1998.
25. **Priit Sarv.** High resolution solid-state NMR studies of zeolites. Tartu, 1998.
26. **Сергей Долгов.** Электронные возбуждения и дефектообразование в некоторых оксидах металлов. Тарту, 1998.
27. **Kaupo Kukli.** Atomic layer deposition of artificially structured dielectric materials. Tartu, 1999.
28. **Ivo Heinmaa.** Nuclear resonance studies of local structure in $RBa_2Cu_3O_{6+x}$ compounds. Tartu, 1999.
29. **Aleksander Shelkan.** Hole states in CuO_2 planes of high temperature superconducting materials. Tartu, 1999.
30. **Dmitri Nevedrov.** Nonlinear effects in quantum lattices. Tartu, 1999.
31. **Rein Ruus.** Collapse of 3d (4f) orbitals in 2p (3d) excited configurations and its effect on the x-ray and electron spectra. Tartu, 1999.
32. **Valter Zazubovich.** Local relaxation in incommensurate and glassy solids studied by Spectral Hole Burning. Tartu, 1999.
33. **Indrek Reimand.** Picosecond dynamics of optical excitations in GaAs and other excitonic systems. Tartu, 2000.
34. **Vladimir Babin.** Spectroscopy of exciton states in some halide macro- and nanocrystals. Tartu, 2001.
35. **Toomas Plank.** Positive corona at combined DC and AC voltage. Tartu, 2001.
36. **Kristjan Leiger.** Pressure-induced effects in inhomogeneous spectra of doped solids. Tartu, 2002.
37. **Helle Kaasik.** Nonperturbative theory of multiphonon vibrational relaxation and nonradiative transitions. Tartu, 2002.
38. **Tõnu Laas.** Propagation of waves in curved spacetimes. Tartu, 2002.
39. **Rünno Lõhmus.** Application of novel hybrid methods in SPM studies of nanostructural materials. Tartu, 2002.
40. **Kaido Reivelt.** Optical implementation of propagation-invariant pulsed free-space wave fields. Tartu, 2003.
41. **Heiki Kasemägi.** The effect of nanoparticle additives on lithium-ion mobility in a polymer electrolyte. Tartu, 2003.
42. **Villu Repän.** Low current mode of negative corona. Tartu, 2004.
43. **Алексей Котлов.** Оксианионные диэлектрические кристаллы: зонная структура и электронные возбуждения. Tartu, 2004.
44. **Jaak Talts.** Continuous non-invasive blood pressure measurement: comparative and methodological studies of the differential servo-oscillometric method. Tartu, 2004.
45. **Margus Saal.** Studies of pre-big bang and braneworld cosmology. Tartu, 2004.

46. **Eduard Gerškevitš.** Dose to bone marrow and leukaemia risk in external beam radiotherapy of prostate cancer. Tartu, 2005.
47. **Sergey Shchemelyov.** Sum-frequency generation and multiphoton ionization in xenon under excitation by conical laser beams. Tartu, 2006.
48. **Valter Kiisk.** Optical investigation of metal-oxide thin films. Tartu, 2006.
49. **Jaan Aarik.** Atomic layer deposition of titanium, zirconium and hafnium dioxides: growth mechanisms and properties of thin films. Tartu, 2007.
50. **Astrid Rekker.** Colored-noise-controlled anomalous transport and phase transitions in complex systems. Tartu, 2007.
51. **Andres Punning.** Electromechanical characterization of ionic polymer-metal composite sensing actuators. Tartu, 2007.
52. **Indrek Jõgi.** Conduction mechanisms in thin atomic layer deposited films containing TiO_2. Tartu, 2007.
53. **Aleksei Krasnikov.** Luminescence and defects creation processes in lead tungstate crystals. Tartu, 2007.
54. **Küllike Rägo.** Superconducting properties of MgB_2 in a scenario with intra- and interband pairing channels. Tartu, 2008.
55. **Els Heinsalu.** Normal and anomalously slow diffusion under external fields. Tartu, 2008.
56. **Kuno Kooser.** Soft x-ray induced radiative and nonradiative core-hole decay processes in thin films and solids. Tartu, 2008.
57. **Vadim Boltrushko.** Theory of vibronic transitions with strong nonlinear vibronic interaction in solids. Tartu, 2008.
58. **Andi Hektor.** Neutrino Physics beyond the Standard Model. Tartu, 2008.
59. **Raavo Josepson.** Photoinduced field-assisted electron emission into gases. Tartu, 2008.
60. **Martti Pärs.** Study of spontaneous and photoinduced processes in molecular solids using high-resolution optical spectroscopy. Tartu, 2008.
61. **Kristjan Kannike.** Implications of neutrino masses. Tartu, 2008.
62. **Vigen Issahhanjan.** Hole and interstitial centres in radiation-resistant MgO single crystals. Tartu, 2008.
63. **Veera Krasnenko.** Computational modeling of fluorescent proteins. Tartu, 2008.
64. **Mait Müntel.** Detection of doubly charged higgs boson in the CMS detector. Tartu, 2008.
65. **Kalle Kepler.** Optimisation of patient doses and image quality in diagnostic radiology. Tartu, 2009.
66. **Jüri Raud.** Study of negative glow and positive column regions of capillary HF discharge. Tartu, 2009.
67. **Sven Lange.** Spectroscopic and phase-stabilisation properties of pure and rare-earth ions activated ZrO_2 and HfO_2. Tartu, 2010.
68. **Aarne Kasikov.** Optical characterization of inhomogeneous thin films. Tartu, 2010.
69. **Heli Valtna-Lukner.** Superluminally propagating localized optical pulses. Tartu, 2010.

70. **Artjom Vargunin.** Stochastic and deterministic features of ordering in the systems with a phase transition. Tartu, 2010.
71. **Hannes Liivat.** Probing new physics in e+e− annihilations into heavy particles via spin orientation effects. Tartu, 2010.
72. **Tanel Mullari.** On the second order relativistic deviation equation and its applications. Tartu, 2010.
73. **Aleksandr Lissovski.** Pulsed high-pressure discharge in argon: spectroscopic diagnostics, modeling and development. Tartu, 2010.
74. **Aile Tamm.** Atomic layer deposition of high-permittivity insulators from cyclopentadienyl-based precursors. Tartu, 2010.
75. **Janek Uin.** Electrical separation for generating standard aerosols in a wide particle size range. Tartu, 2011.
76. **Svetlana Ganina.** Hajusandmetega ülesanded kui üks võimalus füüsikaõppe efektiivsuse tõstmiseks. Tartu, 2011
77. **Joel Kuusk.** Measurement of top-of-canopy spectral reflectance of forests for developing vegetation radiative transfer models. Tartu, 2011.
78. **Raul Rammula**. Atomic layer deposition of HfO_2 – nucleation, growth and structure development of thin films. Tartu, 2011.
79. **Сергей Наконечный.** Исследование электронно-дырочных и интерстициал-вакансионных процессов в монокристаллах MgO и LiF методами термоактивационной спектроскопии. Тарту, 2011.
80. **Niina Voropajeva.** Elementary excitations near the boundary of a strongly correlated crystal. Tartu, 2011.
81. **Martin Timusk.** Development and characterization of hybrid electro-optical materials. Tartu, 2012, 106 p.
82. **Merle Lust.** Assessment of dose components to Estonian population. Tartu, 2012, 84 p.
83. **Karl Kruusamäe.** Deformation-dependent electrode impedance of ionic electromechanically active polymers. Tartu, 2012, 128 p.
84. **Liis Rebane.** Measurement of the $W \to \tau\nu$ cross section and a search for a doubly charged Higgs boson decaying to τ-leptons with the CMS detector. Tartu, 2012, 156 p.
85. **Jevgeni Šablonin.** Processes of structural defect creation in pure and doped MgO and NaCl single crystals under condition of low or super high density of electronic excitations. Tartu, 2013, 145 p.
86. **Riho Vendt**. Combined method for establishment and dissemination of the international temperature scale. Tartu, 2013, 108 p.
87. **Peeter Piksarv.** Spatiotemporal characterization of diffractive and non-diffractive light pulses. Tartu, 2013, 156 p.
88. **Anna Šugai.** Creation of structural defects under superhigh-dense irradiation of wide-gap metal oxides. Tartu, 2013, 108 p.
89. **Ivar Kuusik.** Soft X-ray spectroscopy of insulators. Tartu, 2013, 113 p.
90. **Viktor Vabson**. Measurement uncertainty in Estonian Standard Laboratory for Mass. Tartu, 2013, 134 p.

91. **Kaupo Voormansik.** X-band synthetic aperture radar applications for environmental monitoring. Tartu, 2014, 117 p.
92. **Deivid Pugal.** hp-FEM model of IPMC deformation. Tartu, 2014, 143 p.
93. **Siim Pikker.** Modification in the emission and spectral shape of photostable fluorophores by nanometallic structures. Tartu, 2014, 98 p.
94. **Mihkel Pajusalu**. Localized Photosynthetic Excitons. Tartu, 2014, 183 p.
95. **Taavi Vaikjärv.** Consideration of non-adiabaticity of the Pseudo-Jahn-Teller effect: contribution of phonons. Tartu, 2014, 129 p.
96. **Martin Vilbaste.** Uncertainty sources and analysis methods in realizing SI units of air humidity in Estonia. Tartu, 2014, 111 p.
97. **Mihkel Rähn.** Experimental nanophotonics: single-photon sources- and nanofiber-related studies. Tartu, 2015, 107 p.
98. **Raul Laasner.** Excited state dynamics under high excitation densities in tungstates. Tartu, 2015, 125 p.
99. **Andris Slavinskis.** EST Cube-1 attitude determination. Tartu, 2015, 104 p.
100. **Karlis Zalite**. Radar Remote Sensing for Monitoring Forest Floods and Agricultural Grasslands. Tartu, 2016, 124 p.
101. **Kaarel Piip.** Development of LIBS for *in-situ* study of ITER relevant materials. Tartu, 2016, 93 p.
102. **Kadri Isakar.** ^{210}Pb in Estonian air: long term study of activity concentrations and origin of radioactive lead. Tartu, 2016, 107 p.
103. **Artur Tamm.** High entropy alloys: study of structural properties and irradiation response. Tartu, 2016, 115 p.
104. **Rasmus Talviste.** Atmospheric-pressure He plasma jet: effect of dielectric tube diameter. Tartu, 2016, 107 p.
105. **Andres Tiko.** Measurement of single top quark properties with the CMS detector. Tartu, 2016, 161 p.
106. **Aire Olesk.** Hemiboreal Forest Mapping with Interferometric Synthetic Aperture Radar. Tartu, 2016, 121 p.
107. **Fred Valk.** Nitrogen emission spectrum as a measure of electric field strength in low-temperature gas discharges. Tartu, 2016, 149 p.
108. **Manoop Chenchiliyan.** Nano-structural Constraints for the Picosecond Excitation Energy Migration and Trapping in Photosynthetic Membranes of Bacteria. Tartu, 2016, 115p.
109. **Lauri Kaldamäe.** Fermion mass and spin polarisation effects in top quark pair production and the decay of the higgs boson. Tartu, 2017, 104 p.
110. **Marek Oja.** Investigation of nano-size α- and transition alumina by means of VUV and cathodoluminescence spectroscopy. Tartu, 2017, 89 p.
111. **Viktoriia Levushkina**. Energy transfer processes in the solid solutions of complex oxides. Tartu, 2017, 101 p.
112. **Mikk Antsov**. Tribomechanical properties of individual 1D nanostructures: experimental measurements supported by finite element method simulations. Tartu, 2017, 101 p.